Available online at www.sciencedirect.com
ScienceDirect
Icarus 185 (2006) 39–63
ICARUS
www.elsevier.com/locate/icarus

Shape, size and multiplicity of main-belt asteroids I. Keck Adaptive Optics survey

F. Marchis [a,*], M. Kaasalainen [b], E.F.Y. Hom [c], J. Berthier [d], J. Enriquez [a], D. Hestroffer [d], D. Le Mignant [e], I. de Pater [a]

[a] *Department of Astronomy, University of California, 601 Campbell Hall, Berkeley, CA 94720-3411, USA*
[b] *Department of Mathematics and Statistics, Gustaf Hallstromin katu 2b, P.O. Box 68, FIN-00014 University of Helsinki, Finland*
[c] *Graduate Group in Biophysics, University of California–San Francisco, Genentech Hall, 600, 16th Street, San Francisco, CA 94143-2240, USA*
[d] *IMCCE, UMR-CNRS 8028, Observatoire de Paris, 77 Av. Denfert Rochereau, F-75014 Paris, France*
[e] *W.M. Keck Observatory, 65-1120 Mamalahoa Hwy, Kamuela, HI 96743, USA*

Received 3 April 2006; revised 25 May 2006

Available online 7 August 2006

Abstract

This paper presents results from a high spatial resolution survey of 33 main-belt asteroids with diameters >40 km using the Keck II Adaptive Optics (AO) facility. Five of these (45 Eugenia, 87 Sylvia, 107 Camilla, 121 Hermione, 130 Elektra) were confirmed to have satellite. Assuming the same albedo as the primary, these moonlets are relatively small (∼5% of the primary size) suggesting that they are fragments captured after a disruptive collision of a parent body or captured ejecta due to an impact. For each asteroid, we have estimated the minimum size of a moonlet that can positively detected within the Hill sphere of the system by estimating and modeling a 2-σ detection profile: in average on the data set, a moonlet located at $2/100 \times R_{\mathrm{Hill}}$ ($1/4 \times R_{\mathrm{Hill}}$) with a diameter larger than 6 km (4 km) would have been unambiguously seen. The apparent size and shape of each asteroid was estimated after deconvolution using a new algorithm called AIDA. The mean diameter for the majority of asteroids is in good agreement with IRAS radiometric measurements, though for asteroids with a $D < 200$ km, it is underestimated on average by 6–8%. Most asteroids had a size ratio that was very close to those determined by lightcurve measurements. One observation of 104 Klymene suggests it has a bifurcated shape. The bi-lobed shape of 121 Hermione described in Marchis et al. [Marchis, F., Hestroffer, D., Descamps, P., Berthier, J., Laver, C., de Pater, I., 2005c. Icarus 178, 450–464] was confirmed after deconvolution. The ratio of contact binaries in our survey, which is limited to asteroids larger than 40 km, is surprisingly high (∼6%), suggesting that a non-single configuration is common in the main-belt. Several asteroids have been analyzed with lightcurve inversions. We compared lightcurve inversion models for plane-of-sky predictions with the observed images (9 Metis, 52 Europa, 87 Sylvia, 130 Elektra, 192 Nausikaa, and 423 Diotima, 511 Davida). The AO images allowed us to determine a unique photometric mirror pole solution, which is normally ambiguous for asteroids moving close to the plane of the ecliptic (e.g., 192 Nausikaa and 52 Europa). The photometric inversion models agree well with the AO images, thus confirming the validity of both the lightcurve inversion method and the AO image reduction technique.

Keywords: Asteroids; Infrared observations; Asteroids, surfaces; Data reduction techniques; Image processing

1. Introduction

Considering the existence of the Kuiper belt objects orbiting at $a > 40$ AU and on the scale of our Solar System, the main-belt of asteroids located between Mars and Jupiter ($a =$ 2–4 AU) is very close to Earth. Until recently, little was known about the size, shape, and surface composition of most main-belt asteroids. Even details on the surface of 1 Ceres, the largest main-belt asteroid discovered by G. Piazzi in January 1801 with

* Corresponding author.
E-mail addresses: fmarchis@berkeley.edu (F. Marchis), mjk@rni.helsinki.fi (M. Kaasalainen), erikhom@cgl.ucsf.edu (E.F.Y. Hom), berthier@imcce.fr (J. Berthier), jenriquez@astron.berkeley.edu (J. Enriquez), hestroffer@imcce.fr (D. Hestroffer), davidl@keck.hawaii.edu (D. Le Mignant), imke@berkeley.edu (I. de Pater).

0019-1035/$ – see front matter
doi:10.1016/j.icarus.2006.06.001

a $D \sim 1000$ km (corresponding to an angular diameter at opposition of ∼0.7 arcsec), remain unresolved by ground-based telescopic observations due to angular resolution limitation by the atmospheric turbulence of 0.6–1.2 arcsec. At this angular resolution, only a handful of asteroids can be disk-resolved. Knowledge of the shapes of large asteroids in the main-belt is important because they result from a complex collisional history. Most of them are formed as a result of catastrophic collisions, which also lead to various interesting internal structures that can be categorized into coherent, fractured, or rubble-pile structures (Britt et al., 2002). The overall shape of an asteroid may also correspond to its equilibrium figure (Farinella et al., 1981, 1982).

Most of our knowledge about the shape and size of main-belt asteroids is provided by global photometric measurements. Size can be roughly estimated by measuring the absolute reflecting flux of the asteroids in visible light. Assuming, however, that the albedo of an asteroid's surface can vary from 4% for the Trojan asteroids (Fernández et al., 2003) up to 35% for 4 Vesta (Gaffey et al., 1989), reflectance-based size determination can be uncertain by a factor two. The measurement of the Far-IR (10–200 μm) flux of 2228 asteroids using the IRAS satellite (Tedesco et al., 2002) has provided a good estimate of asteroid radiometric diameters. A more accurate estimate of an asteroid's size and projected shape can be retrieved during stellar occultation. In this case, the mobilization of several observers distributed along the path of the occultation will provide an instantaneous measurement of the apparent shape of the asteroids [e.g., the occultation of 1-Vulpeculae by 2 Pallas in 1983 involving 250 observers in Dunham et al. (1990)]. If occultation analysis is combined with photometric variation measurements produced by the spin of an asteroid, a good approximation of its projected shape can be retrieved [e.g., for 85 Io in Erikson et al. (1999)]. These techniques provide an instantaneous measurement of the 2D projected shape of an asteroid. To obtain an estimate of the full 3D shape, several measurements sampling the full rotation of the asteroid (if possible) are necessary.

Photometric lightcurves can provide a good estimate of the 3D shape of an asteroid. They are major source of information for all asteroid populations, from the near-Earth asteroids (Kaasalainen et al., 2004) to the Kuiper Belt (Sheppard and Jewitt, 2004). Kaasalainen et al. (2001) developed a powerful inversion method for determining the shape, rotation period, and pole direction, as well as the scattering law of several asteroids based on their lightcurves. Using this inversion method on ∼100 asteroids for which a large number of well-sampled lightcurves were available, Kaasalainen and co-workers showed that 3D shape irregularities, more than albedo structure, are the major sources of small lightcurve variations seen in visible (see Kaasalainen et al., 2004 and references therein). As shown in Ďurech and Kaasalainen (2003), photometric data are seldom sufficient for resolving nonconvex shape features. Thus the detailed modeling of double/bifurcated asteroids requires complementary data sources such as AO (Kaasalainen and Lamberg, 2006).

With the recent upgrades at the Arecibo radar telescope, additional large asteroids can be probed in the main-belt. Using this telescope, Ostro et al. (2000) estimated the shape of 216 Kleopatra and confirmed a bifurcated structure suggested by Adaptive Optics (AO) observations (Marchis et al., 1999; Hestroffer et al., 2002). On recent thought very rare encounters, interplanetary spacecrafts have been used to image main-belt asteroids. Very accurate images of 951 Gaspra (Thomas et al., 1994), and 243 Ida (Belton et al., 1994) taken by the Galileo mission, 5535 Annefrank with the Stardust spacecraft (Duxbury et al., 2004), and 25143 Itokawa by Hayabusa spacecraft (Fujiwara et al., 2006) confirm highly irregular shapes for main-belt asteroids and offer clues on the process by which they are formed.

Adaptive optics correct in real-time for the atmospheric turbulence and provide diffraction-limited near-infrared images. Such systems are now available on most 8–10 m telescopes. Their performance scales with the wavelength of observation and the brightness of the reference star. Most of the recent results obtained by this technique focused on the search and analysis of secondary moonlet previously discovered around 18 main-belt asteroids. Our group focused on constraining the companion orbits of several systems: 22 Kalliope (Marchis et al., 2003b), 45 Eugenia (Marchis et al., 2004b), 87 Sylvia (Marchis et al., 2005b), 90 Antiope (Descamps et al., 2005), to name a few. These analyses provided information about the formation of those binary asteroids and gave clues about their interior structure. The design and performance of AO systems have continued to mature, so as to provide more stable correction on fainter targets. It is now possible by ground-based AO instrumentation to resolve several main-belt asteroids which are very close to the diffraction limit of an 8–10 m telescope (typically ∼60 mas, corresponding to main-belt asteroids with $D > 50$ km), enabling us to study the size and shape of small asteroids (e.g., Conrad et al., 2003; Marchis et al., 2004b, 2005a, 2005b, 2005c) and to map the surface of larger asteroids (e.g., 4 Vesta; Zellner et al., 2005).

We report in this study an analysis of our survey of main-belt asteroids. This first article is dedicated to the observations performed using the Keck II AO system. We describe in detail the observations and the data-processing applied in Section 2. In Section 3, we describe the analysis of the data focusing on the criteria for the detection of moonlet companions and present an estimate of their size and shape. In Section 4, we compare the apparent shape of sub-sample of 7 asteroids with the results from the lightcurve inversion method. In the final section, we compare our calculated size and shape with either IRAS size measurements or lightcurve data, for asteroids that do not have accurate 3D shape models.

2. Observations and data processing

2.1. Collected data

In 2001, we initiated a campaign to identify and study binary asteroids in various populations of asteroids from the main-belt to the trans-neptunian objects using telescopes equipped with AO systems (Marchis et al., 2004a). The data presented here were collected in 2003 and 2004 using the Keck II AO sys-

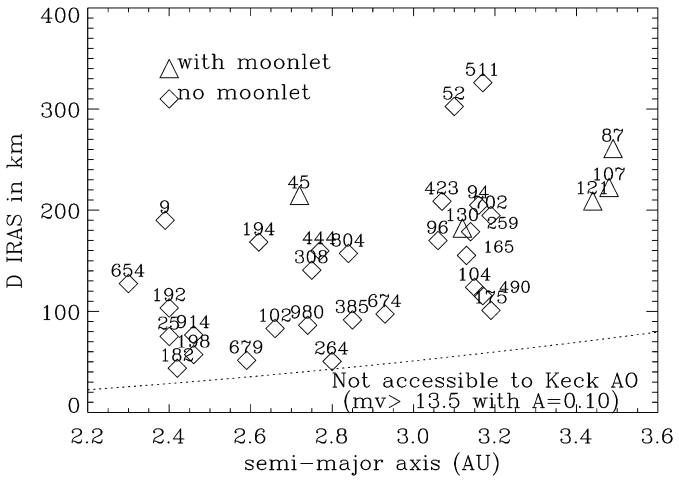

Fig. 1. Distribution of our targets in size (IRAS diameter) as a function of the semi-major axis of their orbit. Considering a limit for the wavefront sensor analyzer of 13.5 magnitude in the visible, approximately 250–300 main-belt targets are observable with the Keck AO system.

tem (Wizinowich et al., 2000) and the near-infrared NIRC-2 camera (1024 × 1024 Aladdin-3 InSb array). All observations were recorded in the narrow field of view (with a 9.942 mas pixel scale) in Kp broad-band filter ($\lambda_0 = 2.124$ μm; $\Delta\lambda = 0.351$ μm). The AO system was used in Natural-Guide Star (NGS) mode, i.e., the asteroid itself was used as a reference for the AO wavefront sensor. With the improvements made to the system in 2003 (van Dam et al., 2004), the Keck AO system is able to provide full and stable correction in this mode for targets up to $R = 13.5$ magnitude under good atmospheric conditions (photometric sky and seeing $< 0.8''$), reaching a Strehl Ratio of ∼45% in Kp band.

Because of their small predicted angular size ($<0.2''$), the main-belt asteroids are excellent targets for an AO system. Fig. 1 illustrates the sensitivity limits of the wavefront sensor as function of distance to the Sun. Our selected targets are well-above this limit. By estimating the magnitude in visible and using the IMCCE ephemeris,[1] we find that a total of ∼300 main-belt asteroids (with perihelia > 2.15 AU and aphelia < 3.3 AU) should be accessible to the Keck AO system in its NGS mode. This survey focuses on observations covering 11% of this total. For each observing night, we selected from the IMCCE ephemeris all asteroids with an elongation angle larger than 120° and a predicted magnitude in the visible $m_v < 13.8$. A typical sample would include approximately 110 asteroid candidates. The total typical integration time per asteroid is ∼5 min. Considering the overhead of the telescope and the AO system, the number of targets observable on a 5 h half-night was ∼20 (Marchis et al., 2004a). Thirty eight observations of 31 main-belt asteroids are reported in Tables 1a and 1b on three half-nights (December 6, 2003, December 7, 2003, and October 25, 2004).

Two additional observations are included in this work: 192 Nausikaa, observed in September 2000 at its opposition using KCAM camera in H broad band filter ($\lambda_0 = 1.63$ μm; $\Delta\lambda = 0.30$ μm). One observation of 511 Davida recorded in Kp band with NIRC-2 in December 2002 (Conrad et al., 2003) is also included in our analysis. Most of the targets were observed close to their opposition at an average distance of ∼1.9 AU. Their mean estimated size from Tedesco et al. (2002) varied from 43 to 326 km (Fig. 1).

Basic data processing (sky substraction, bad-pixel removal, and flat-field correction) was applied on the raw data using the *eclipse* data reduction package (Devillard, 1997). Successive frames taken over a time span less than 8 min, were combined into one single averaged image after applying an accurate shift-and-add transformation through the *Jitter* pipeline[2] offered in the same package. Data processing with this software on such high S/N data (∼1000) is relatively straightforward, since the centroid position on each frame is estimated by a Gaussian fit, then the final image is obtained stacking set of cross-correlated individual frames.

2.2. Image quality

AO systems enable real-time observations with an angular resolution close to the diffraction limit of the telescope. The quality of AO correction, however, can vary slightly in time due to variations in seeing conditions during a night and as a function of target brightness. To better characterize the quality of the Keck AO data during our observations, we recorded several observations of unresolved stars at similar magnitudes (between magnitude 9 and 12.8) several times during the nights, and used them as approximations to the point spread function (PSF) of the AO system. The quality of correction can be estimated either by measuring the full width half-maximum (FWHM) on the star, corresponding to the angular resolution of the image, or calculating the Strehl ratio (SR), which compares the observational PSF with the theoretical PSF provided by the telescope.[3] The characteristics of these PSF stars is described in Table 2. It is important to note that the AO corrections are stable in this wavelength range and for these bright targets. The FWHM which is estimated to be ∼54 mas (for a SR ∼ 35%), is quite close to the diffraction limit of the telescope (43 mas at 2.1 μm) and corresponds to a spatial resolution of 75 km at 1.9 AU (the average distance of the targets in this survey).

2.3. Deconvolution

The typical PSF in adaptive optics is characterized by a peak of coherent light that defines the spatial resolution surrounded by a halo produced by the uncorrected residual phase. The direct effect of this halo is a blurring of the recorded image. As we measured an estimate of the AO system PSF, it is possible to apply an a posteriori deconvolution method to improve image sharpness. Deconvolution is an inversion process which

[1] Institut de Mécanique Céleste et de Calculs des Éphémerides, Paris, France, http://www.immce.fr.

[2] Devillard, N., 1999, available on http://www.eso.org/projects/dfs/papers/jitter99/.

[3] A SR = 100% corresponds to a perfect correction; in Kp band without AO correction SR ∼ 2–4%.

Table 1a
Observation log of the Keck AO survey for the targets observed in the years 2000, 2002, and 2003

ID#	Name	Filter	Inttime (s)	Sequence numbers	Date	UT	PSF	Mag. (eph.)	Distance (AU)	Elongation (deg)
192	Nausikaa1	H	40	18–38	2000-Sep-16	10:59:03	PSFNausikaa	9.5	0.93234408	138
192	Nausikaa2	H	205	113–144	2000-Sep-16	12:07	PSFNausikaa	9.5	0.93207997	138
192	Nausikaa3	H	86	160–210	2000-Sep-16	12:35	PSFNausikaa	9.5	0.93197048	138
511	Davida	Kp	150	581–595	2002-Dec-27	11:05	PSFNausikaa	9.6	1.61718893	172
804	Hispania	Kp	360	22–27	2003-Dec-06	05:41:06	–	12.4	2.01684642	115
423	Diotima	Kp	360	31–38	2003-Dec-06	06:01:39	–	12.7	2.57330370	113
264	Libussa	Kp	360	40–48	2003-Dec-06	06:18:29	–	12.6	1.77020359	120
121	Hermione	Kp	90	229–237	2003-Dec-06	12:30:12	–	12.7	2.56999707	141
45	Eugenia	Kp	45	238–246	2003-Dec-06	12:42:35	–	12.3	2.14009619	125
702	Alauda	Kp	56	247–255	2003-Dec-06	12:55:45	–	12.1	2.32724833	158
104	Klymene	Kp	75	256–270	2003-Dec-06	13:08:51	–	12.1	1.74537897	161
25	Phocaea	Kp	45	271–285	2003-Dec-06	13:25:14	–	12.2	1.93474448	148
385	Ilmatar	Kp	180	286–291	2003-Dec-06	13:45:51	–	11.8	1.90300548	137
121	Hermione2	Kp	720	292–300	2003-Dec-06	14:03:38	–	12.7	2.56960678	141
45	Eugenia2	Kp	180	301–303	2003-Dec-06	14:20:55	–	12.3	2.13928771	125
194	Prokne	Kp	540	01–09	2003-Dec-07	04:49:17	PSFRachele	11.8	1.73466110	111
198	Ampella	Kp	540	11–19	2003-Dec-07	05:13:22	PSFRachele	11.5	1.26944149	126
980	Anacostia	Kp	540	20–28	2003-Dec-07	05:33:14	PSFRachele	11.7	1.55579352	132
674	Rachele	Kp	540	29–37	2003-Dec-07	05:55:14	PSFRachele	11.8	1.86856377	127
198	Ampella2	Kp	360	38–43	2003-Dec-07	06:12:31	PSFRachele	11.5	1.26987290	126
674	Rachele2	Kp	540	53–61	2003-Dec-07	06:53:00	PSFRachele	11.8	1.86892617	127
130	Elektra	Kp	540	62–70	2003-Dec-07	07:16:55	PSFRachele	11.0	1.73829496	138
679	Pax	Kp	240	71–74	2003-Dec-07	07:32:53	PSFRachele	11.6	1.07084191	130
52	Europa	Kp	180	77–79	2003-Dec-07	07:50:15	PSFRachele	11.1	2.19881868	133
121	Hermione	Kp	720	352–354	2003-Dec-07	12:39:13	PSFHermione	12.7	2.56243968	142
102	Miriam	Kp	420	367–369	2003-Dec-07	13:07:24	PSFHermione	12.5	1.45750237	166
104	Klymene	Kp	360	374–380	2003-Dec-07	13:24:58	PSFHermione	12.1	1.74168348	162
308	Polyxo	Kp	360	381–386	2003-Dec-07	13:38:52	PSFHermione	12.4	1.92463994	154
444	Gyptis	Kp	360	387–392	2003-Dec-07	13:54:42	PSFHermione	12.8	2.30953193	124
94	Aurora	Kp	360	393–398	2003-Dec-07	14:28:17	PSFHermione	12.6	2.31423187	124

Notes. 192 Nausikaa is the only asteroid observed with the KCAM IR camera. For the other satellites, we used NIRC-2 IR camera which was commissioned at the end of the year 2001. Kp and H broadband filters are centered at 2.12 and 1.63 μm with a bandwidth of 0.34 and 0.30 μm, respectively. On December 6, 2003, we did not record a PSF star and we later used a combination of PSFRachele & PSFHermione taken on December 7 for the deconvolution algorithm.

Table 1b
Observation log for the asteroids observed in 2004

Num	Name	Filter	Inttime (s)	Frames	Date	UT	PSF	Mag. (eph.)	Distance (AU)	Elongation (deg)
9	Metis	Kp	360	56–61	2004-Oct-25	06:00:38	PSFMetis	9.9	1.47259510	132
87	Sylvia	Kp	180	65–66	2004-Oct-25	06:29:16	PSFMetis/PSFT2	12.4	2.59045768	121
175	Andromache	Kp	180	68–70	2004-Oct-25	06:39:57	PSFMetis/PSFT2	12.4	1.73037755	127
107	Camilla	Kp	180	71–72	2004-Oct-25	06:53:31	PSFT2	13.0	2.88340878	132
96	Aegle	Kp	180	74–75	2004-Oct-25	07:03:51	PSFT2/T3	13.0	2.56333733	145
914	Palisana	Kp	180	77–79	2004-Oct-25	07:15:55	PSFT2/PSFT3	12.1	1.36352098	141
9	Metis2	Kp	180	91–96	2004-Oct-25	08:01:37	PSFT3/PSFT2	9.9	1.47326231	132
654	Zelinda	Kp	180	97–98	2004-Oct-25	08:17:09	PSFT3/PSFGR2	12.4	1.47803855	146
259	Aletheia	Kp	180	100–101	2004-Oct-25	08:29:11	PSFT3/PSFGR2	12.9	2.38771057	144
490	Veritas	Kp	180	103–105	2004-Oct-25	08:40:45	PSFT2/PSFGR2	12.7	1.94414461	151
165	Loreley	Kp	180	106–108	2004-Oct-25	09:04:16	PSFGR2	12.3	2.15711784	155
182	Elsa	Kp	180	113–117	2004-Oct-25	09:44:34	PSFGR2	11.6	1.09346795	154

aims to reconstruct a good approximation for the initial object given the PSF for the system. Many algorithms based on different mathematical approaches for both astronomical instrumentation as well as medical imaging have been developed in the last two decades (Starck et al., 2002). Part of our group is involved in the development of a deconvolution method dedicated to objects with well-defined edge, a common characteristic to spatially-resolved planetary science targets. Our new adaptive image deconvolution algorithm (AIDA) which is described and tested thoroughly in Hom et al. (2006) is based on a stochastic approach to the deconvolution problem. The algorithm, inspired by MISTRAL (Myopic Iterative STep-preserving Restoration ALgorithm), a deconvolution algorithm developed by Mugnier et al. (2004), includes several important improvements. This new algorithm aims to find the best image reconstruction, using information about the object and the PSF. It requires several star

Table 2
Characteristic of the PSF stars recorded during the runs

PSF name	Date	Official name	RA_{J2000} hh:mm:ss	DEC_{J2000} dd:mm:ss	m_v	FWHM mas
PSFNausikaa	2000-Sep-16	HD 12593	02:03:47.0	+19:17:31.7	9.2	43
PSFDavida	2002-Dec-27	TY2-13399331	06:51:49.9	+19:17:41.8	10.7	51
PSFRachele	2003-Dec-07	TY2-31751	01:30:45.5	+02:53:38.6	11.7	53
PSFHermione	2003-Dec-07	TY2-19192151	07:38:04.4	+26:21:33	12.8	52
PSFMetis	2004-Oct-25	TY2-5827981	23:15:21.6	−13:21:26.3	9.3	51
PSFT2	2004-Oct-25	TY2-17206481	23:36:08.5	+15:26:38.9	12.2	57
PSFT3	2004-Oct-25	TY2-11755601	23:33:11.3	+14:01:53.8	12.2	56
PSFGR2	2004-Oct-25	TY2-118219271	00:21:02.8	+19:42:24	11.2	55

Notes. At the end of 2003, the Keck AO system was upgraded. It provides now a stable correction with an angular resolution very close to the diffraction limit of the telescope for targets up to the 13th magnitude. It is therefore not necessary to record a PSF star for each target.

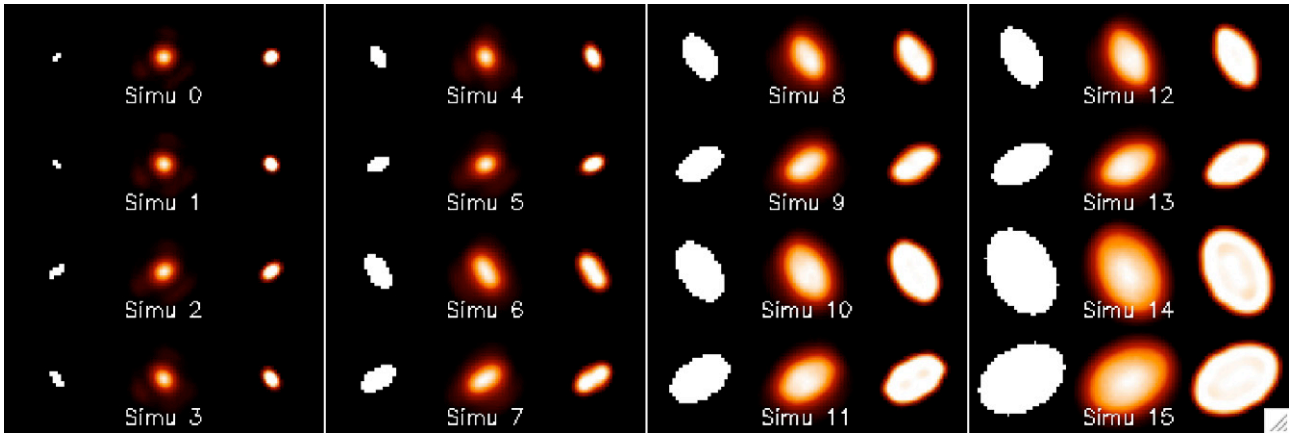

Fig. 2. Simulation of deconvolution with AIDA for various asteroid sizes. For each of them, the perfect initial asteroid is displayed, follows by the convolved and noisy image. The last frame corresponds to the image after deconvolution. The peak S/N of the convolved images is ∼1300 which mimics our observations quite well. For the largest asteroids, some deconvolved images still show a typical bright-edge artifact with a contrast <15%.

images to evaluate variations in the PSF. The main improvement of this approach over more classical methods is that it avoids both noise amplification and the creation of sharp-edged artifacts or "ringing effects," and thus better restores the photometry (see simulations below). Additionally, we implemented in AIDA an automatic determination of the balance between the maximum-likelihood criterion and two regularization priors. The first one called L1–L2 permits the restoration of a sharp edge in the image limiting the formation of Gibbs artifacts close to the limb of the asteroid. The second is the myopic criterion which considers the variability of the PSF. How the algorithm weights each prior to achieve a good deconvolution is beyond the scope of this paper and is described in Hom et al. (2006). An inappropriate weighting of the L1–L2 prior, made manually by the user in MISTRAL, can result in strong Gibbs artifacts. For instance, this problem is apparent in deconvolved images of 511 Davida presented in Conrad et al. (2003).

To characterize the performance of the AIDA deconvolution for the study of shape and size of main-belt asteroids, we performed a series of simulations: artificial images of asteroids with various sizes (from 2 to 20 pixels), shapes (an ellipse whose axis ratio $a/b = 1.0, 1.2, \ldots, 2.0$), and orientations were created. These perfect images were degraded by convolving them with one real set of observed PSFs from Table 2. Both Poisson and detector noises were added to the degraded image for which the peak S/N was ∼1200, hence mimicking the image quality in our observations. The AIDA deconvolution was applied on these sets of images using its adaptive regularization weighting, and using a different set of PSFs to better quantify the effect of variability of the AO correction. Fig. 2 displays one set with various sizes, two orientations, and the same a/b ratio. The deconvolution process improves the sharpness of the image and restores the initial shape and orientation of the images for an asteroid larger than >5 pixels. For the largest asteroids, some deconvolved images still show a typical bright-edge artifact with a contrast <10–15%. A feature at lower contrast could be in fact an artifact of deconvolution. To measure the size, the apparent shape, and the orientation of an asteroid, we fit the image with an ellipse characterized by a major axis $2a$, a minor axis $2b$ and the orientation (in degrees counter-clockwise from the sky east). We compared these parameters with the ones defined to build the initial image for the simulation.

We summarized in Fig. 3 a statistical study of the size recovery accuracy for the entire set of simulations. In this figure, we compared the ratio between the measured size before and after deconvolution with that of the initial image. For a size between 5 and 12 pixels (corresponding to 50–120 mas), the estimated size after deconvolution is better on average (with an accuracy of ∼5–10%) than before deconvolution (usually over-estimated by 10–30%). Beyond 12 pixel size, the differ-

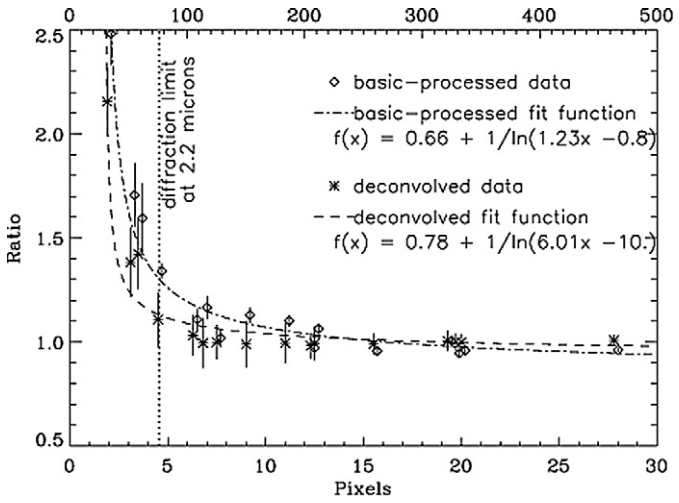

Fig. 3. Accuracy of the size recovery for the basic-processed and deconvolved data. The gain in the size determination after deconvolution with AIDA is significant for 5 to 10 pixel size asteroids. Below the diffraction limit of the Keck-10m telescope in Kp band, the size of the asteroid cannot be recovered precisely. An empirical log-based function was fit to estimate the accuracy. It will be used in our analysis to estimate the uncertainties on the size determination for any asteroid.

ence between the size measurements on the basic-processed and deconvolved images is less evident although the accuracy on a deconvolved image is 3% better. Below 5 pixels, which corresponds to the angular resolution provided by the Keck AO system (see Section 2.2), the estimation of the real size of the asteroid is challenging even after deconvolution. To quantify the accuracy of our size estimates for the asteroids in our sample (see Section 3.1), we fit the ratio in Fig. 3 by an empirical function.

3. Analysis of the data

3.1. Shape and size

The AIDA deconvolution algorithm was applied to all basic-processed frames of asteroid listed in Tables 1a and 1b. To better estimate the PSF variability, in several cases (e.g., for December 6, 2003) we used as an initial set of PSF, a mixed set of PSF frames taken the day after or on the same day as the observations. Owing to the excellent stability of the AO correction as described in Section 2.2, this approximation has a minor impact on the final deconvolved image which is clearly improved as shown in Figs. 4a–4e. The deconvolution is not perfect and could be improved by slightly tuning the regularization parameters. However most of the work described here aims to estimate the size and shape of the asteroids. Our simulations ensured a good calibration of the systematic effects affecting the size estimate, caused by AIDA when it is ran with standard automatic parameters. Considering that this calibration could be affected by a manual adjustment of the parameters, and that the size and shape determination is the main goal of this study, we did not

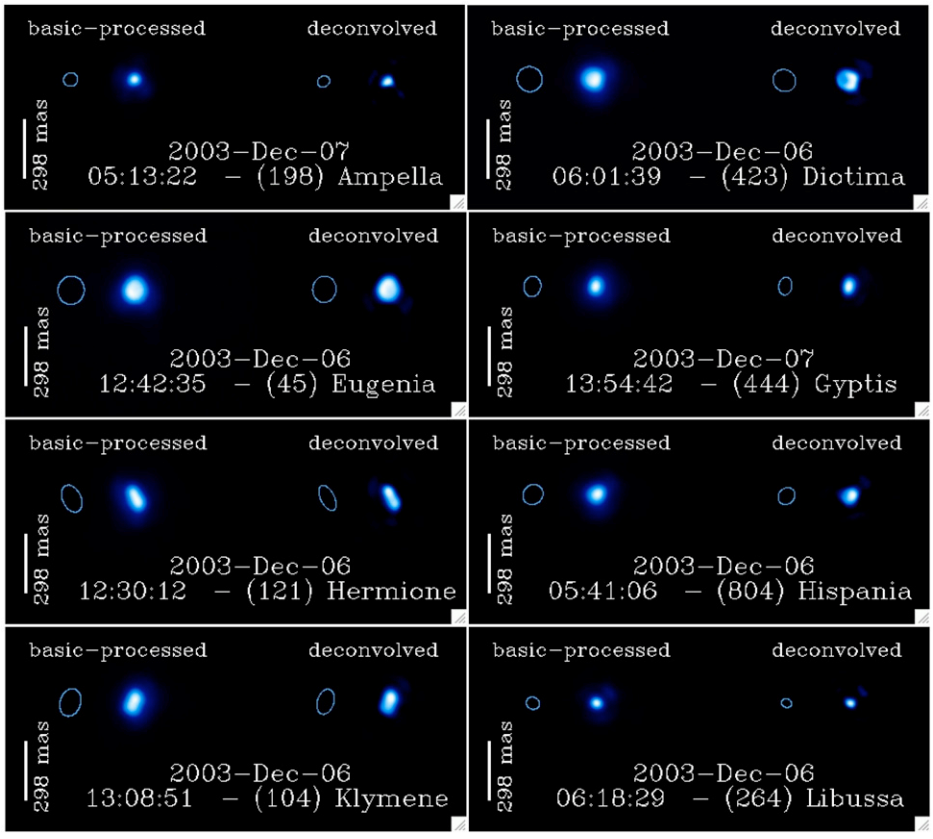

(a)

Fig. 4. Main-belt asteroids observed with Keck AO system. On the left column, the basic processed image is displayed. The right column corresponds to the deconvolved image.

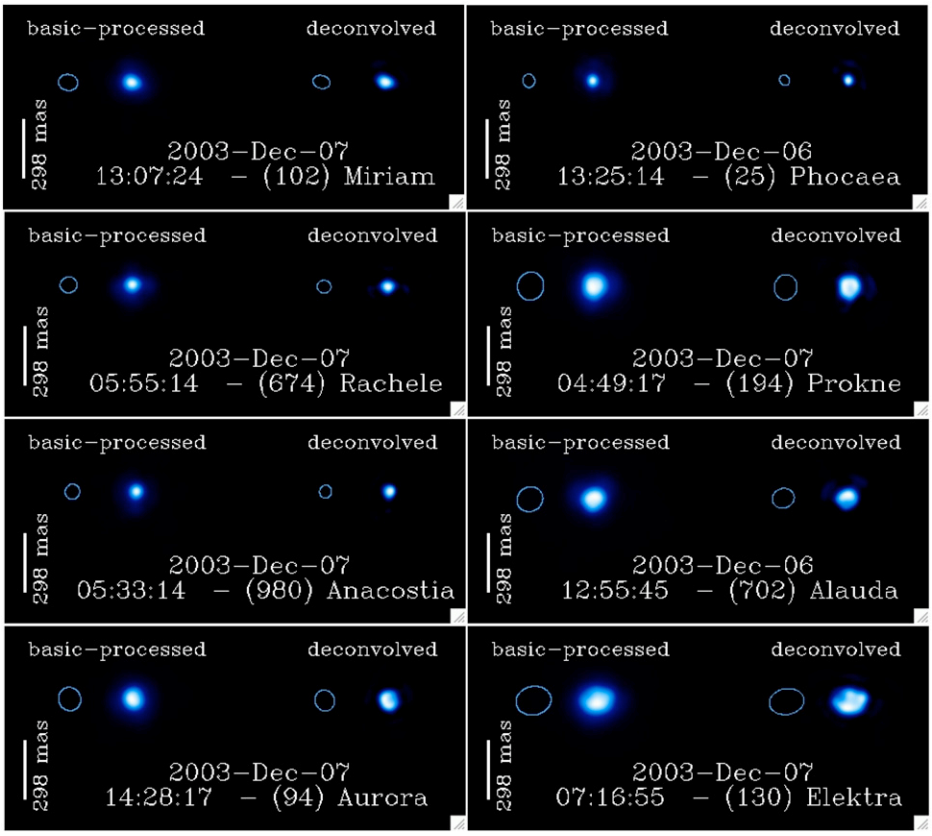

(b)

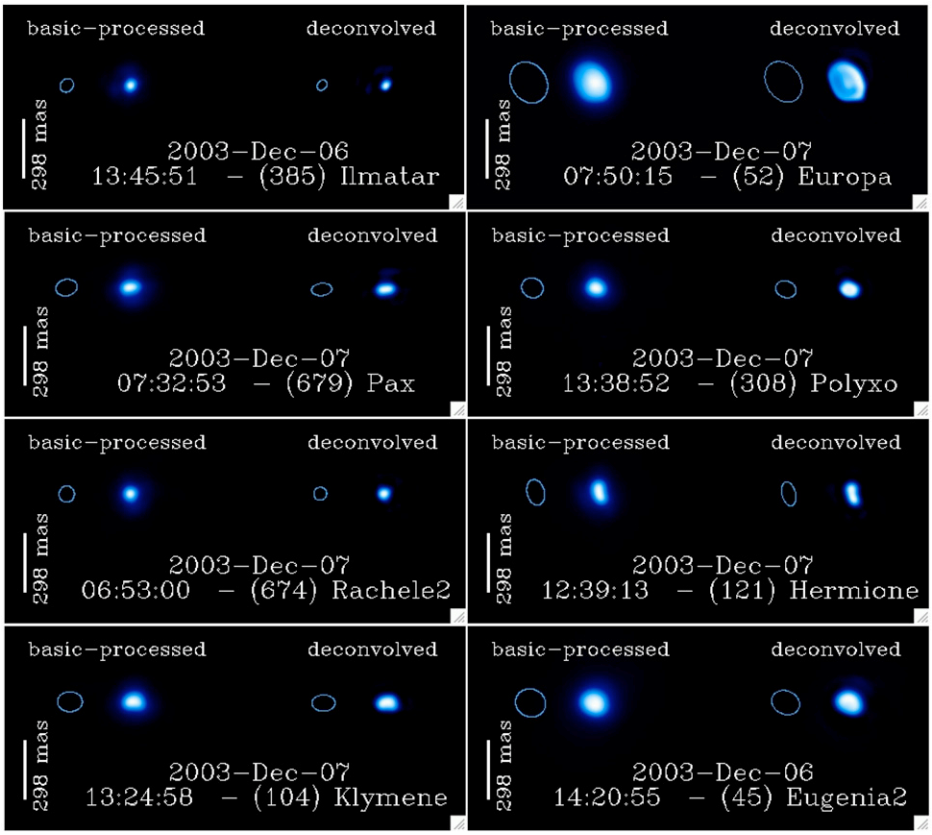

(c)

Fig. 4. (*continued*)

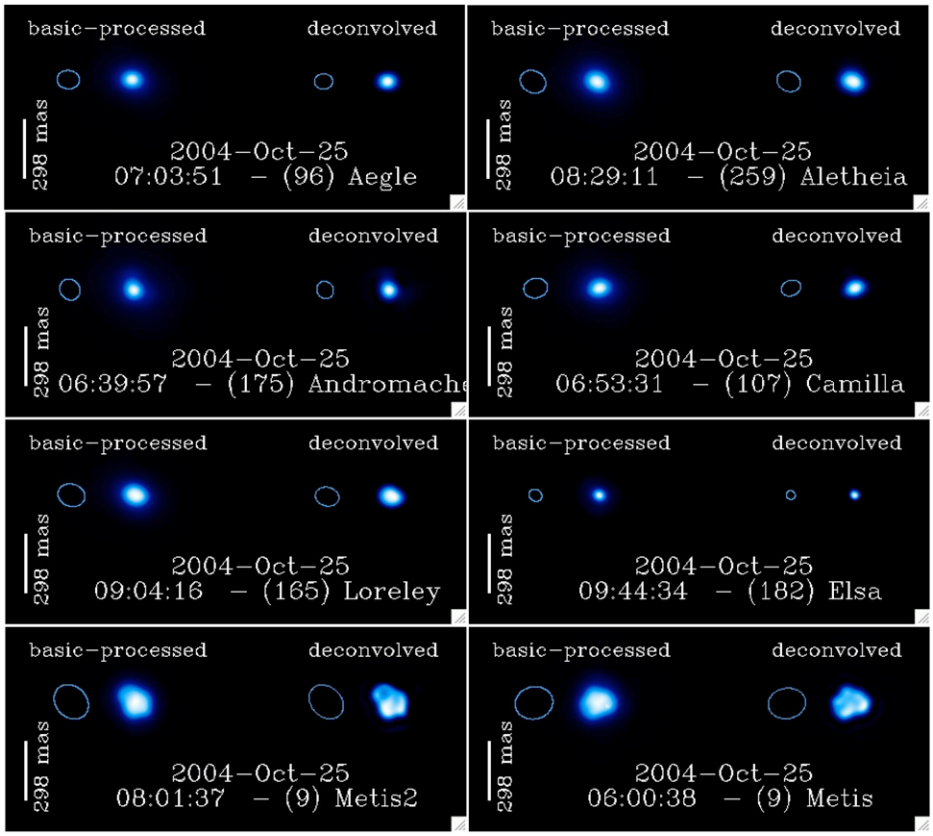

(d)

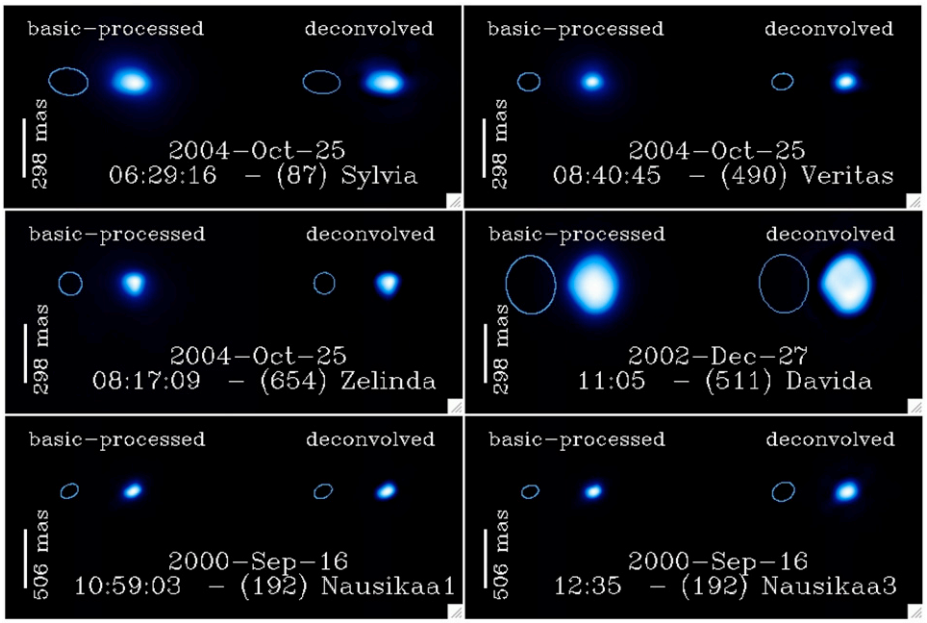

(e)

Fig. 4. (*continued*)

perform a manual optimization in each case, thereby favoring the accuracy of the size determination.

The size and shape were approximated using the same fitting technique described for the simulated images in Section 2.3. For comparison, we also fit an ellipse on the basic-processed images. The major-axes and orientations obtained for both, the basic-processed and the deconvolved images, are listed in Tables 3a and 3b. A brief comparison between the size measurements confirm that those obtained from the basic-processed data are over-estimated in comparison with the deconvolved ones. This effect is predominant for the asteroids with a major-axis between 5 and 10 pixels.

Table 3a
Determination of the apparent size and orientation of the asteroids observed between 2000 and 2003

Date	UT time	Target	Basic-processed					Deconvolved				
			Angle (deg)	2*a* (mas)	2*b* (mas)	2*a* (km)	2*b* (km)	Angle (deg)	2*a* (mas)	2*b* (mas)	2*a* (km)	2*b* (km)
2000-Sep-16	10:59:03	Nausikaa1	118.7	151	101	102	68	118.0	154	103	104	69
2000-Sep-16	12:35	Nausikaa3	109.2	138	99	93	67	118.7	185	143	125	97
2002-Dec-27	11:05	Davida	−265.1	294	247	345	290	−264.9	295	244	346	287
2003-Dec-06	12:55:45	Alauda	34.5	132	121	223	205	19.2	110	97	186	164
2003-Dec-06	06:01:39	Diotima	−44.7	126	123	236	231	−36.1	116	107	217	200
2003-Dec-06	12:42:35	Eugenia	82.3	142	131	221	204	82.6	131	117	204	181
2003-Dec-06	14:20:55	Eugenia2	−24.8	152	138	236	215	−25.0	143	116	223	181
2003-Dec-06	12:30:12	Hermione	−245.3	143	91	268	170	−243.6	136	67	254	125
2003-Dec-06	14:03:38	Hermione2	84.5	106	89	199	166	83.3	95	70	177	131
2003-Dec-06	05:41:06	Hispania	45.2	105	94	154	138	45.3	90	77	131	113
2003-Dec-06	13:45:51	Ilmatar	56.4	73	61	100	84	51.8	56	43	78	60
2003-Dec-06	13:08:51	Klymene	72.2	141	101	178	128	73.0	129	81	163	103
2003-Dec-06	06:18:29	Libussa	−25.9	66	60	85	77	−17.0	52	42	66	54
2003-Dec-06	13:25:14	Phocaea	−263.6	67	58	95	82	−241.7	54	47	76	66
2003-Dec-07	05:13:22	Ampella	31.2	71	67	65	62	28.4	63	52	58	48
2003-Dec-07	06:12:31	Ampella2	−227.3	71	70	65	64	−266.3	56	53	52	49
2003-Dec-07	05:33:14	Anacostia	74.4	76	71	86	80	76.6	65	59	73	67
2003-Dec-07	14:28:17	Aurora	−248.3	118	110	199	184	−249.9	106	95	178	160
2003-Dec-07	07:16:55	Elektra	10.8	175	143	221	181	9.1	174	129	220	163
2003-Dec-07	07:50:15	Europa	−238.4	217	176	346	280	−235.5	218	167	349	267
2003-Dec-07	13:54:42	Gyptis	80.0	103	84	173	141	80.7	90	64	151	108
2003-Dec-07	12:39:13	Hermione	−256.2	130	86	241	160	−255.9	123	67	229	125
2003-Dec-07	13:24:58	Klymene	−1.2	124	99	157	125	−0.2	115	81	145	103
2003-Dec-07	13:07:24	Miriam	−12.2	95	80	101	85	−15.5	86	65	91	68
2003-Dec-07	07:32:53	Pax	11.4	108	81	83	63	6.2	101	61	78	47
2003-Dec-07	13:38:52	Polyxo	−23.8	108	97	151	136	−19.7	104	82	145	115
2003-Dec-07	04:49:17	Prokne	76.4	142	130	178	164	84.3	127	113	160	142
2003-Dec-07	05:55:14	Rachele	17.0	84	79	114	107	−10.0	69	63	93	86
2003-Dec-07	06:53:00	Rachele2	85.0	81	76	110	103	52.6	66	63	89	86

Notes. The measurement is performed fitting an ellipse (major-axis 2*a*, minor-axis 2*b*) on the basic-processed and the deconvolved final images. The orientation of the major-axis is given in degrees counter-clockwise from the astronomical east.

Table 3b
Determination of the apparent size and orientation of the asteroids observed in 2004

Date	UT time	Target	Basic-processed					Deconvolved				
			Angle (deg)	2*a* (mas)	2*b* (mas)	2*a* (km)	2*b* (km)	Angle (deg)	2*a* (mas)	2*b* (mas)	2*a* (km)	2*b* (km)
2004-Oct-25	07:03:51	Aegle	−5.1	112	92	209	171	2.1	91	77	170	143
2004-Oct-25	08:29:11	Aletheia	−27.3	131	108	227	188	−23.7	122	98	211	170
2004-Oct-25	06:39:57	Andromache	−235.0	109	97	137	121	−232.9	89	81	112	102
2004-Oct-25	06:53:31	Camilla	11.4	119	98	250	206	20.1	100	77	210	161
2004-Oct-25	09:44:34	Elsa	−30.2	68	58	54	46	−29.6	46	42	36	33
2004-Oct-25	09:04:16	Loreley	−17.9	136	111	214	174	−15.5	118	93	185	147
2004-Oct-25	06:00:38	Metis	13.0	189	161	201	172	9.5	188	152	201	162
2004-Oct-25	08:01:37	Metis2	−44.3	188	153	201	163	−44.0	190	148	203	158
2004-Oct-25	07:15:55	Palisana	9.8	99	94	98	93	51.3	83	72	82	71
2004-Oct-25	06:29:16	Sylvia	−8.0	195	135	367	254	−3.9	185	115	348	217
2004-Oct-25	08:40:45	Veritas	4.8	110	92	155	129	11.7	105	81	148	115
2004-Oct-25	08:17:09	Zelinda	30.2	118	114	126	122	77.2	106	104	114	111

Notes. The measurement is performed fitting an ellipse (major-axis 2*a*, minor-axis 2*b*) on the basic-processed and the deconvolved final images. The orientation of the major-axis is given in degrees counter-clockwise from the astronomical east.

In Tables 4a and 4b, we report the best size and shape estimates in km for the 33 asteroids observed in this survey. The error bar reported for the major-axes of the ellipse has been derived from the empirical function obtained from our simulated images after deconvolution as described in Section 2.3. The uncertainty in the orientation was approximated by comparing the results from the fits on the basic-processed and deconvolved images. We are confident that we obtain a good estimate of the uncertainty on the orientation of the fit ellipse, since the Keck AO PSF is quite symmetrical with a $\mathrm{FWHM}_x/\mathrm{FWHM}_y < 5\%$. Therefore, even after convolution by the PSF of the AO system, the asteroid elliptical shape keeps its asymmetry and the un-

Table 4a
Apparent size and orientation of the asteroids observed in 2000–2003

Date	UT time	Target	2*a* (km)	2*b* (km)	Angle (deg)
2003-Dec-06	12:55:45	Alauda	186 ± 6	164 ± 6	26 ± 10
2003-Dec-06	06:01:39	Diotima	217 ± 6	200 ± 6	40 ± 4
2003-Dec-06	12:42:35	Eugenia	204 ± 4	181 ± 5	82 ± 1
2003-Dec-06	14:20:55	Eugenia2	223 ± 3	181 ± 5	−24 ± 1
2003-Dec-06	12:30:12	Hermione	254 ± 4	125 ± 9	−244 ± 1
2003-Dec-06	14:03:38	Hermione2	177 ± 7	131 ± 9	83 ± 1
2003-Dec-06	05:41:06	Hispania	131 ± 6	113 ± 7	45 ± 1
2003-Dec-06	13:45:51	Ilmatar	78 ± 7	60 ± 8	54 ± 3
2003-Dec-06	13:08:51	Klymene	163 ± 3	103 ± 5	72 ± 1
2003-Dec-06	06:18:29	Libussa	66 ± 7	54 ± 8	−21 ± 6
2003-Dec-06	13:25:14	Phocaea	76 ± 8	66 ± 8	−252 ± 15
2003-Dec-07	05:13:22	Ampella	58 ± 4	48 ± 5	29 ± 1
2003-Dec-07	06:12:31	Ampella2	52 ± 5	49 ± 5	−246 ± 27
2003-Dec-07	05:33:14	Anacostia	73 ± 6	67 ± 6	75 ± 1
2003-Dec-07	14:28:17	Aurora	178 ± 6	160 ± 7	−249 ± 1
2003-Dec-07	07:16:55	Elektra	220 ± 1	163 ± 3	9 ± 1
2003-Dec-07	07:50:15	Europa	349 ± 2	267 ± 1	−236 ± 2
2003-Dec-07	13:54:42	Gyptis	151 ± 7	108 ± 8	80 ± 1
2003-Dec-07	12:39:13	Hermione	229 ± 5	125 ± 9	−256 ± 1
2003-Dec-07	13:24:58	Klymene	145 ± 4	103 ± 5	0 ± 1
2003-Dec-07	13:07:24	Miriam	91 ± 4	68 ± 5	−13 ± 2
2003-Dec-07	07:32:53	Pax	78 ± 3	47 ± 4	8 ± 3
2003-Dec-07	13:38:52	Polyxo	145 ± 5	115 ± 6	−21 ± 2
2003-Dec-07	04:49:17	Prokne	160 ± 3	142 ± 4	80 ± 5
2003-Dec-07	05:55:14	Rachele	93 ± 7	86 ± 7	3 ± 19
2003-Dec-07	06:53:00	Rachele2	89 ± 7	86 ± 7	68 ± 22

Notes. The error bars on the size measurements is estimated considered the simulation performed after deconvolution (see Section 2.3) and using the empirical law displayed in Fig. 2.

Table 4b
Apparent size and orientation of the asteroids observed in 2004

Date	UT time	Target	2*a* (km)	2*b* (km)	Angle (deg)
2004-Oct-25	07:03:51	Aegle	170 ± 8	143 ± 9	−1 ± 5
2004-Oct-25	08:29:11	Aletheia	211 ± 5	170 ± 7	−25 ± 2
2004-Oct-25	06:39:57	Andromache	112 ± 5	102 ± 5	−233 ± 1
2004-Oct-25	06:53:31	Camilla	210 ± 8	161 ± 10	15 ± 6
2004-Oct-25	09:04:16	Loreley	185 ± 5	147 ± 6	−16 ± 1
2004-Oct-25	06:00:38	Metis	201 ± 1	162 ± 1	11 ± 2
2004-Oct-25	08:01:37	Metis2	203 ± 1	158 ± 2	−44 ± 1
2004-Oct-25	07:15:55	Palisana	82 ± 4	71 ± 5	30 ± 29
2004-Oct-25	06:29:16	Sylvia	348 ± 1	217 ± 6	−5 ± 2
2004-Oct-25	08:40:45	Veritas	148 ± 5	115 ± 6	8 ± 4
2004-Oct-25	08:17:09	Zelinda	114 ± 4	111 ± 4	54 ± 23
2002-Dec-27	11:05	Davida	346 ± 7	287 ± 3	−265 ± 1
2000-Sep-16	10:59:03	Nausikaa1	104 ± 4	69 ± 5	118 ± 1
2000-Sep-16	12:35	Nausikaa3	125 ± 3	97 ± 4	113 ± 6

Notes. The error bars on the size measurements is estimated considered the simulation performed after deconvolution (see Section 2.3) and using the empirical law displayed in Fig. 2.

certainty on the orientation is mostly introduced by the fitting process.

3.2. Search for moonlet companions

3.2.1. Upper limit on moonlet detection

The search for faint sources in the vicinity of an asteroid is a nontrivial task. The PSF of the Keck AO consists of a coherent peak surrounded by a halo in which speckle patterns are also visible (Figs. 5a and 5b). These patterns, which are produced by mutual interference of partially coherent light, are subject to minute temporal and spatial fluctuations in relation to the seeing conditions, the brightness of the AO source, and its airmass. In the specific case of the Keck telescope whose mirror is composed of 36 hexagonal 1.8-m segments, surface errors at the center of each segment ("dimples") and discontinuities at segment edges may be the source of quasi-static speckle-type artifacts in a regular pattern. Because these speckle artifacts naturally have the size of the diffraction-limited telescope image (Perrin et al., 2003) and have faint intensity ($\Delta m > 7$), they could be mistaken for moonlet satellites, thus complicating this search program.

Inspired by an algorithm to search for faint companions around B-type stars (Shatsky and Tokovinin, 2002), we developed a method to reduce the halo effect and estimate the upper limit of detection for our AO observations. This analysis was performed on the basic-processed images (see Section 2.1) since the use of a deconvolution method is not appropriate to detect a low S/N point source. This algorithm was initially developed to quantify the minimum size of possible moonlets orbiting Trojan asteroids. This previous observing program was performed using various AO systems and related technologies (NGS, LGS, appulses) which provided data of variable quality (Marchis et al., 2004a).

For each frame, $P(r,\theta)$, the azimuthally averaged profile $P(r) = \langle P(r,\theta)\rangle_\theta$ was calculated. This azimuthally averaged image was subtracted from the image itself: $f(r) - P(r,\theta) - \langle P(r,\theta)\rangle_\theta$. A detection threshold of 2-$\sigma(r)$ was set, where $\sigma(r)$ is the rms of the azimuthal intensity fluctuations $f(r) = \langle f(r,\theta)\rangle_\theta$. Since the detection functions $[f(r)]$ for each asteroid have common characteristics, they can be approximated by fitting them to two linear functions. For $r < r_{\rm lim}$ and $r > 0.2''$, they are roughly proportional to a log function ($f(r) = \alpha \times \log(r)$) with α typically between -9 and -4. In this regime, the Poisson noise and residual speckle noise dominate the signal, which is the reason why the detection function varies log-linearly with the distance from the asteroid centroid. The parameter α is directly related to the angular size of the light peak, and is therefore associated with the angular size of the asteroid and the intrinsic quality of the AO correction. For $r > r_{\rm lim}$ the detection function is constant with $f(r) = \Delta m_{\rm lim}$; $\Delta m_{\rm lim}$ is directly proportional to the integration time and varies from -9.1 to -6.5, the typical limit of detection for a ∼5 min integration in the Kp broadband filter.

Figs. 5a and 5b illustrate each step of the analysis. 45 Eugenia was the first binary system discovered from the ground (Merline et al., 1999). We observed this binary asteroid system on December 6, 2003 at 2 different epochs. Subtracting the azimuthally averaged function improved the detection of Petit–Prince, the companion of 45 Eugenia. In the range of $r < 0.2$ arcsec, however, the detection is limited ($\Delta m < -4$) mostly due to (i) the asymmetry of the PSF wings, (ii) the presence of speckle noise, and (iii) the elongation of the resolved primary itself. Between 0.2 and 0.5 arcsec, the 2-σ detection function is linear with a coefficient of $\alpha = -6.1$ and reaching $\Delta m = -7.5$ at 0.6 arcsec. A transition in detection occurs

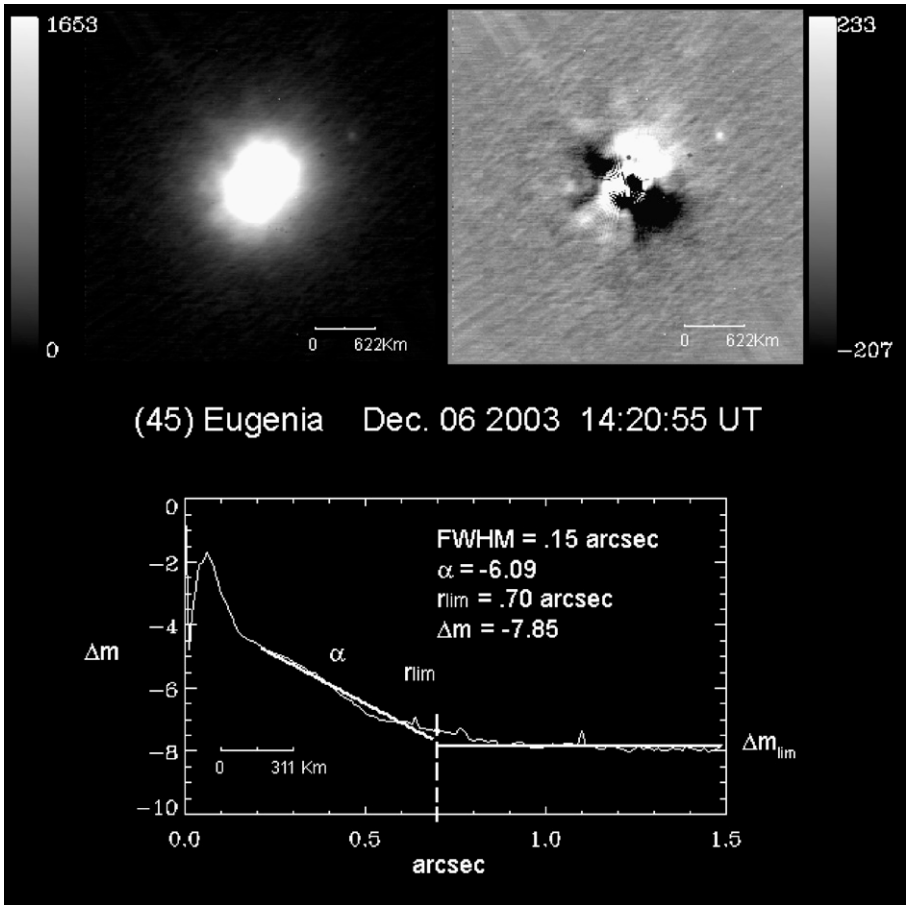

(a)

Fig. 5. (a) Search for moonlets around 45 Eugenia. On the left-top figure an observation of 45 Eugenia taken on December 6, 2003 is displayed. The right-top figure corresponds to the same observations after subtracting its azimuthal average. The detection of the moonlet companion is easier. The plot below is the 2-σ detection function for this observation. It is approximated using 2 linear functions which depends of 3 parameters: α, the coefficient of the slope in the linear regime, $\Delta m_{\rm lim}$ the difference of magnitude in the stable area, and $r_{\rm lim}$ the separation between both regimes. The minimum size of a moonlet to be detected can be derived. (b) Search for moonlets around 423 Diotima. On the left-top figure an observation of 423 Diotima taken on December 6, 2003 is displayed. The right-top figure corresponds to the same observations after subtraction its azimuthal average. No moonlet companion are detected around this asteroid. The plot below is the 2-σ detection function for this observation. It is slightly different than 45 Eugenia detection function because of the variability of the AO correction (which depends on the brightness of the reference and the seeing conditions).

between 0.6 and 0.8 arcsec. Beyond ∼0.80 arcsec ($r_{\rm lim}$), corresponding to a distance of 1230 km from 45 Eugenia (2.1 AU), the detection limit remains constant with $\Delta m_{\rm lim} \sim -7.8$. Considering the size of Eugenia [$D_{\rm IRAS} = 215$ km in Tedesco et al. (2002)] and the pixel scale of the NIRC2 (9.94 mas), we calculate that a moonlet with a diameter ∼6 km should be detectable in the stable regime. Hence, Petit–Prince, located 0.75″ from the primary, was clearly detected with a Δm(peak-to-peak) $= -5.6$, corresponding to a 7 km diameter moonlet assuming the same albedo for the moon and primary. This system will be carefully analyzed using additional observations taken with the VLT-8m AO system (Marchis et al., 2004b) and Gemini Archive (Marchis et al., 2006; in preparation).

The same analysis performed on 423 Diotima, which was observed on the same night, is presented in Fig. 5b. The detection function does not display the same characteristics than the Eugenia's one because the brightness of Diotima, its airmass, and seeing conditions were different. This asteroid has a predicted ephemeris magnitude of $m_v = 12.7$. For $r > 0.2$ arcsec, the speckle noise was still significant even after subtracting the azimuthally averaged function. The speckle patterns are clearly visible on the subtracted image. The detection function reaches -7.7 magnitude beyond $r_{\rm lim} = 0.55$ arcsec. In this regime, a moonlet with a size larger than 5.9 km should be detectable. Despite the existence of a companion suggested by Schober (1983), none was detected around 423 Diotima.

For each frame, the detection function was calculated and synthesized. The function parameters are labeled in Tables 6a and 6b. The average values of the synthetic parameters for all the observations were $\alpha = -5.6 \pm 1.3$, $\Delta m_{\rm lim} = -8.0 \pm 0.6$, and $r_{\rm lim} = 0.64 \pm 0.14$. Since the brightness of the reference (the asteroid itself) on the wavefront analyzer of the AO system and the integration time for most of the targets were of the same order, the $\Delta m_{\rm lim}$ was relatively stable. The parameter α, which corresponds to the angular resolution, varied because the angular size of the asteroids was different. We performed the same analysis for similar magnitude asteroids observed using the

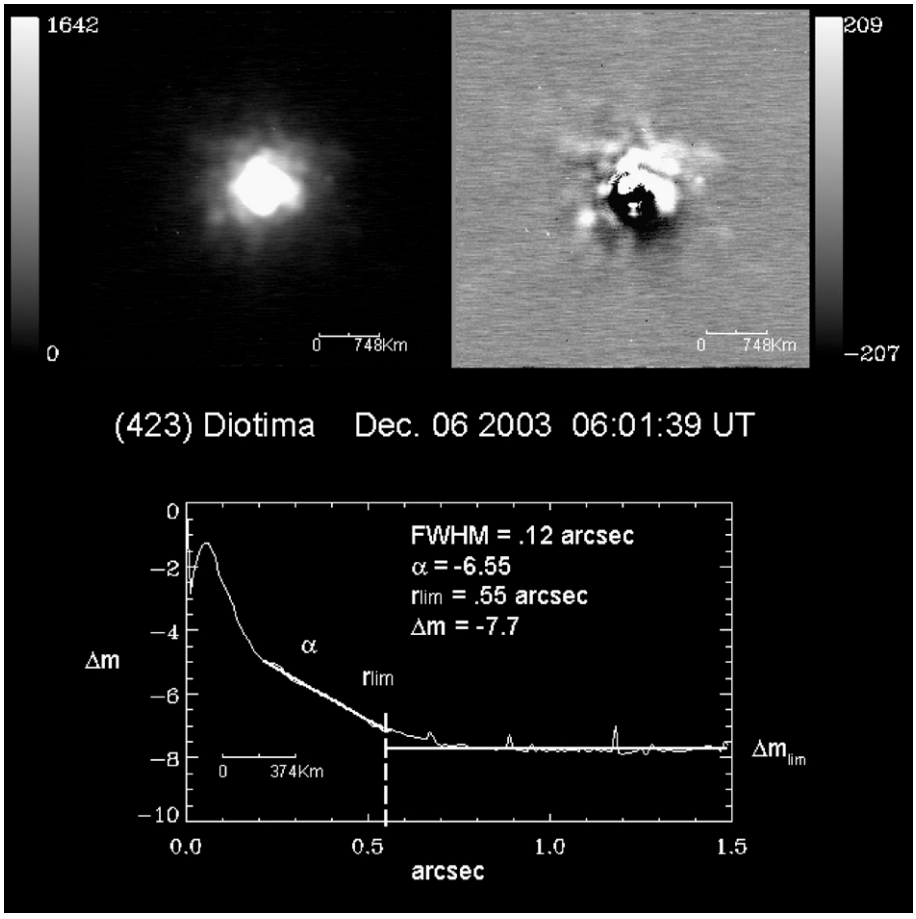

(b)

Fig. 5. (*continued*)

VLT-8m AO system (NACO) and with the Lick-3m LGS AO system. The VLT-NACO system provides a similar averaged detection function for 12–14 magnitude targets. For the Lick LGS, however, the angular resolution is 2–4 times worst leading to a significantly lower sensitivity ($\alpha = -4$, $\Delta m_{\rm lim} = -6$, and $r_{\rm lim} = 2$).

Only a dozen over approximately ∼80 known main-belt moonlet binary systems are well characterized. An accurate determination of the orbital parameters of such system require a long term program of observations spanning several years. This task was initiated a few years ago by our group; and we have thus far measured the orbits of 22 Kalliope and Linus (Marchis et al., 2003a), 45 Eugenia and Petit–Prince (Marchis et al., 2004b), 87 Sylvia and its two moonlets (Marchis et al., 2005b) and 121 Hermione and "LaFayette" [proposed name for S/2002 (121) 1] (Marchis et al., 2005c). Additional estimated orbits for the companions of 107 Camilla, 379 Huenna, and 3749 Balam have been proposed by Marchis et al. (2005a). From the measurements of the semi-major axis and the period of revolution of the secondary moonlet, the mass of the system can be inferred. The Hill radius [$R_{\rm Hill} = a(m/3M_{\rm Sun})^{1/3}$ with semi-major axis, a, and mass of the primary, m] corresponds to the radius of a sphere in which the gravitational field of the asteroid is larger than the one produced by the Sun. Within the Hill Sphere, a moonlet with a circular orbit and low inclination will have a stable orbit. For the 22, 45, 87, and 121 binary asteroid systems, we find that moonlet orbiting at $\sim\frac{2}{100} \times R_{\rm Hill}$, well inside the Hill sphere. In contrast, the 3749 Balam and 379 Huenna asteroid systems have loosely bound moonlet companion with semi-major axis values of $\sim\frac{1}{4} \times R_{\rm Hill}$ and $\sim\frac{1}{8} \times R_{\rm Hill}$, respectively (Marchis et al., 2005a). In Tables 6a and 6b, we calculated the Hill radius for each asteroid and estimated their mass, based on their IRAS diameter and assumed the following average densities: 1.7 g/cm^3 for C-type and additional sub-class (B, F, and G) asteroids, and 2.4 g/cm^3 for S-type asteroids (Birlan, 2002); for M-type asteroids, we chose an average density of 3.5 g/cm^3 based on direct measurements reported in Ostro et al. (2000) and Hestroffer et al. (2002) for 216 Kleopatra and in Marchis et al. (2003b) and Margot (2002) for 22 Kalliope.

Using estimates of $R_{\rm Hill}$ for each asteroid, the limits of detection (in diameter magnitude and in diameter) for moonlet at $\frac{2}{100} \times R_{\rm Hill}$ and at $\frac{1}{4} \times R_{\rm Hill}$ were derived. Tables 6a and 6b report the result of these calculations for each asteroid observation. On average, it should be possible to detect a moonlet orbiting at $\frac{2}{100} \times R_{\rm Hill}$ ($\frac{1}{4} \times R_{\rm Hill}$) with a diameter of ∼6 km (∼4 km) using the Keck AO system. None of our observations showed the presence of a loosely bound companion around these >40 km asteroids, even though we had the capability of detecting a fragment ∼10–50 times smaller than the primary.

Table 5
Summary of the mean sizes and axes ratios for the asteroids our survey

Asteroids	$D_{\text{aver.}}$ (km)	D_{IRAS} (km)	Keck AO(a/b) measured	LC(a/b) max	Rotation rate (h)	Comments
9 Metis	181	∼190	1.28 ± 0.03	1.39	5.079	Irregular shape + surface features
25 Phocaea	71	75.1	1.15 ± 0.14	1.18	9.945	Resolved
45 Eugenia	202	214.6	1.23 ± 0.05	1.46	5.699	Elongated + companion
52 Europa	308	302	1.30 ± 0.01	1.20	5.633	Elliptical shape + surface features
87 Sylvia	282	260.9	1.60 ± 0.05	1.77	5.184	Elongated + companion
94 Aurora	169	204.9	1.11 ± 0.08	1.12	7.22	Resolved
96 Aegle	156	169.9	1.19 ± 0.12	1.12	13.82	Resolved
102 Miriam	79	83.0	1.34 ± 0.15	1.16	15.789	Elongated
104 Klymene	133	123.7	1.58 ± 0.10	1.32	8.984	Bifurcation suggested
107 Camilla	185	222.6	1.30 ± 0.13	1.61	4.8439	Elongated + companion
121 Hermione	189	209	2.03 ± 0.16	1.51	5.551	Bi-lobated + companion
130 Elektra	191	182.3	1.35 ± 0.03	1.71	5.225	Elongated + companion
165 Loreley	166	155	1.26 ± 0.08	1.15	7.226	Elongated
175 Andromache	107	100.9	1.09 ± 0.09	1.37	7.668	Resolved
182 Elsa	<36	43.7	–	1.91	80.0	Not resolved
192 Nausikaa	86	103.3	1.51 ± 0.19	1.45	13.622	Elongated
194 Prokne	151	168.4	1.13 ± 0.06	1.28	15.67	Resolved
198 Ampella	53	57.2	1.21 ± 0.19	1.22	10.383	Resolved
259 Aletheia	190	178.6	1.24 ± 0.08	1.19	15.0	Elongated
264 Libussa	60	50.5	1.22 ± 0.36	>1.22	7.056	Resolved
308 Polyxo	130	140.7	1.26 ± 0.11	1.20	12.032	Resolved
385 Ilmatar	69	91.5	1.30 ± 0.30	1.58	62.35	Elongated
423 Diotima	208	208.8	1.08 ± 0.06	1.18	4.775	Resolved
444 Gyptis	129	159.6	1.40 ± 0.16	1.15	6.214	Resolved
490 Veritas	131	115.5	1.29 ± 0.11	1.36	7.930	Elongated
511 Davida	316	326.1	1.21 ± 0.03	1.26	5.1294	Resolved + surface features
654 Zelinda	112	127.4	1.00 ± 0.06	1.32	31.9	Resolved
674 Rachele	89	97.3	1.08 ± 0.18	1.15	30.94	Resolved
679 Pax	62	51.5	1.66 ± 0.23	1.34	8.452	Elongated
702 Alauda	175	194.7	1.13 ± 0.08	1.10	8.36	Resolved
804 Hispania	122	157.2	1.16 ± 0.13	1.25	14.845	Resolved
914 Palisana	76	76.6	1.16 ± 0.14	1.18	15.62	Resolved
980 Anacostia	70	86.2	1.09 ± 0.20	1.10	20.117	Resolved

Notes. The lightcurve size ratio (LC(a/b)) and spin period are extracted from the Minor Planet Lightcurve Parameters updated by A.W. Harris and B.D. Warner (see text for references). The mean size is compared with the radiometric IRAS measurements (Tedesco et al., 2002).

3.2.2. New ideas

The calculation of an upper limit of detection is crucial considering that several groups have been searching for binary asteroids using current AO facilities available on 8-m-class telescopes. The observing time on these telescopes is precious and their efforts could be optimized if the upper limits of detection for the observed targets were also published. In the future, new instruments such as larger ground-based telescopes (>30 m), Adaptive Optics in visible, new space telescopes (JWST, GAIA) may provide a better sensitivity and angular resolution. The publication of previous surveys will help to optimize the target lists for possible new programs to search for moonlet companions.

We are reporting 41 observations of 33 main-belt asteroids with a diameter >40 km. Five of these (45 Eugenia, 87 Sylvia, 107 Camilla, 121 Hermione, 130 Elektra) are already known to have a secondary moonlet, which we confirmed in our Keck survey (see Fig. 15). Considering directly the angular size of the primary measured on the AO images (Tables 4a and 4b), the relative integrated flux (calculated by aperture photometry both on the primary and the moonlet) and assuming the same albedo, we estimated the moonlet diameter in Table 7. In average, the moonlet is 5% smaller than the primary. The proportion of binary asteroids in this survey is quite high (∼15%) but were de facto biased since we were also interested in better defining the orbits of known binary asteroids. No second moonlet was obviously detected in any of these known binary systems. To detect a new moonlet at $2/100 \times R_{\text{Hill}}$ ($1/4 \times R_{\text{Hill}}$), its diameter has to be larger than ∼6 km (∼4 km). Out of ∼28 targets observed in this survey, no new binary asteroid system was discovered. Our small Keck sample suggests that the percentage of binary asteroids with $D > 40$ km is less than 4%.

4. Discussion

A total of 33 asteroids were observed in our survey. Three of them, 52 Europa, 87 Sylvia, and 511 Davida are larger than 250 km. We measured the apparent size, the a/b ratio. We also calculated the upper limit of detection for a secondary moonlet at various distances as a function of the Hill radius. Table 5 summarizes the main characteristics of the observations for each

Table 6a
Search for moonlet companions around our sample in 2003

Name	Date–time (UT)	α	$\Delta m_{\rm lim}$	$r_{\rm lim}$	$R_{\rm Hill}$ (km)	At $2/100 \times R_{\rm Hill}$		At $1/4 \times R_{\rm Hill}$	
						Δm	D (km)	Δm	D (km)
192 Nausikaa	2000-Sep-16 10:59:03	−6.9	−7.7	0.31	19,661	−7.7	3.0	−7.9	2.8
192 Nausikaa	2000-Sep-16 12:07	−8.8	−7.7	0.32	19,661	−7.8	2.9	−7.8	2.8
192 Nausikaa	2000-Sep-16 12:35	−7.1	−8.8	0.48	19,661	−8.7	1.9	−8.8	1.8
511 Davida	2002-Dec-27 11:05	−4.5	−7.8	0.72	81,861	−8.4	6.9	−8.1	8.0
804 Hispania	2003-Dec-06 5:41:06	−5.3	−7.9	0.67	35,337	−7.1	6.1	−7.9	4.2
423 Diotima	2003-Dec-06 6:01:39	−6.6	−7.7	0.55	50,732	−7.1	7.8	−7.7	5.9
264 Libussa	2003-Dec-06 6:18:29	−7.8	−9.1	0.60	12,653	−5.6	3.8	−9.1	0.8
121 Hermione	2003-Dec-06 12:30:12	−5.3	−7.1	0.60	56,939	−6.8	9.1	−7.1	7.9
45 Eugenia	2003-Dec-06 12:42:35	−4.4	−6.9	0.51	46,261	−6.7	9.7	−6.9	9.0
702 Alauda	2003-Dec-06 12:55:45	−5.1	−7.2	0.60	49,238	−6.8	8.4	−7.2	7.2
104 Klymene	2003-Dec-06 13:08:51	−4.3	−7.1	0.64	30,918	−6.5	6.2	−7.1	4.6
25 Phocaea	2003-Dec-06 13:25:14	−3.9	−7.6	0.64	16,135	−5.9	5.0	−7.6	2.3
385 Ilmatar	2003-Dec-06 13:45:51	−5.7	−8.6	0.71	20,645	−6.1	5.6	−8.6	1.8
121 Hermione	2003-Dec-06 14:03:38	−6.4	−7.7	0.40	56,939	−7.3	7.2	−7.7	6.1
45 Eugenia	2003-Dec-06 14:20:55	−6.1	−7.8	0.70	46,261	−7.1	8.2	−7.9	5.7
194 Prokne	2003-Dec-07 4:49:17	−4.8	−8.2	0.79	34,907	−7.0	6.7	−8.3	3.7
198 Ampella	2003-Dec-07 5:13:22	−6.2	−9.1	0.65	12,590	−6.1	3.4	−9.2	0.8
980 Anacostia	2003-Dec-07 5:33:14	−6.4	−9.1	0.64	21,154	−6.8	3.8	−9.1	1.3
674 Rachele	2003-Dec-07 5:55:14	−5.6	−8.8	0.77	22,555	−6.5	4.9	−8.8	1.7
198 Ampella	2003-Dec-07 6:12:31	−6.1	−8.9	0.71	12,590	−5.9	3.8	−8.9	1.0
674 Rachele	2003-Dec-07 6:53:00	−4.8	−8.8	0.78	22,555	−6.6	4.6	−8.8	1.7
130 Elektra	2003-Dec-07 7:16:55	−4.1	−8.4	0.84	45,039	−7.7	5.3	−8.5	3.7
679 Pax	2003-Dec-07 7:32:53	−3.7	−8.3	0.79	10,551	−6.3	2.9	−8.3	1.1
52 Europa	2003-Dec-07 7:50:15	−5.0	−7.5	0.67	74,253	−7.2	10.8	−7.6	9.2
121 Hermione	2003-Dec-07 12:39:13	−4.5	−8.2	0.77	56,939	−7.6	6.3	−8.2	4.7
102 Miriam	2003-Dec-07 13:07:24	−5.2	−8.3	0.65	17,494	−6.0	5.2	−8.4	1.8
104 Klymene	2003-Dec-07 13:24:58	−4.4	−8.1	0.78	30,918	−7.3	4.3	−8.1	2.9
308 Polyxo	2003-Dec-07 13:38:52	−5.3	−8.2	0.70	30,642	−7.2	5.1	−7.9	3.7
444 Gyptis	2003-Dec-07 13:54:42	−5.0	−7.7	0.61	35,044	−6.7	7.3	−7.7	4.7
94 Aurora	2003-Dec-07 14:28:17	−4.4	−7.8	0.68	51,339	−7.4	6.7	−7.8	5.6

Notes. The characteristics of the 2-σ detection curve for each asteroid (α is the slope of the function, $r_{\rm lim}$ separation between both noise regimes dominated by the Poisson noise close to the primary at $r < r_{\rm lim}$ and by the [detector + sky] noises at $r > r_{\rm lim}$. At $r > r_{\rm lim}$ the detection function can be approximated by a flat function with a value of $\Delta m_{\rm lim}$). The radius of the Hill Sphere calculating based on consideration about the size and density of the asteroid (see text) is calculated. The minimum size for a moonlet to be detected at 1/4 and 2/100 $R_{\rm Hill}$ is also indicated.

Table 6b
Search for moonlet companions around our sample in 2004

Name	Date–time (UT)	α	$\Delta m_{\rm lim}$	$r_{\rm lim}$	$R_{\rm Hill}$ (km)	At $2/100 \times R_{\rm Hill}$		At $1/4 \times R_{\rm Hill}$	
						Δm	D (km)	Δm	D (km)
9 Metis	2004-Oct-25 6:00:38	−5.8	−8.2	0.65	35,925	−7.7	5.4	−8.4	4.0
87 Sylvia	2004-Oct-25 6:29:16	−4.9	−7.3	0.84	72,136	−7.0	10.5	−7.3	9.1
175 Andromache	2004-Oct-25 6:39:57	−7.2	−6.5	0.40	25,466	−5.6	7.6	−6.6	4.9
107 Camilla	2004-Oct-25 6:53:31	−6.9	−7.7	0.39	61,345	−6.2	12.7	−7.8	6.0
96 Aegle	2004-Oct-25 7:03:51	−5.4	−8.1	0.72	41,178	−7.1	6.6	−8.1	4.0
914 Palisana	2004-Oct-25 7:15:55	−6.1	−9.0	0.63	14,917	−6.0	4.8	−9.1	1.2
9 Metis	2004-Oct-25 8:01:37	−3.9	−8.3	0.84	35,925	−7.1	7.1	−8.4	4.0
654 Zelinda	2004-Oct-25 8:17:09	−6.1	−8.7	0.72	23,184	−7.3	4.4	−8.8	2.2
259 Aletheia	2004-Oct-25 8:29:11	−6.8	−7.5	0.42	44,436	−6.9	7.6	−7.6	5.4
490 Veritas	2004-Oct-25 8:40:45	−3.7	−7.9	0.85	29,009	−6.6	5.6	−7.9	3.0
165 Loreley	2004-Oct-25 9:04:16	−9.2	−8.4	0.57	38,455	−7.3	5.4	−8.4	3.2
182 Elsa	2004-Oct-25 9:44:34	−6.3	−8.6	0.60	8,366	−5.8	3.0	−8.6	0.8

Notes. The characteristics of the 2-σ detection curve for each asteroid (α is the slope of the function, $r_{\rm lim}$ separation between both noise regimes dominated by the Poisson noise close to the primary at $r < r_{\rm lim}$ and by the [detector + sky] noises at $r > r_{\rm lim}$. At $r > r_{\rm lim}$ the detection function can be approximated by a flat function with a value of $\Delta m_{\rm lim}$). The radius of the Hill Sphere calculating based on consideration about the size and density of the asteroid (see text) is calculated. The minimum size for a moonlet to be detected at 1/4 and 2/100 $R_{\rm Hill}$ is also indicated.

asteroid. 182 Elsa is the only asteroid in our survey which was not resolved by the Keck AO observations. In the case where a target was observed multiple times, we report the observations taken at the maximum apparent size. The averaged measured asteroid size was in good agreement with IRAS radiometric diameters reported by Tedesco et al. (2002). For the 19 out of 30

Table 7
Angular separation, photometric measurement (integrated and peak-to-peak difference in magnitude) between the moonlet and the primary

Name primary	Date–time (UT)	Ang. sep. (in arcsec)	Δ_m (peak-to-peak)	Δ_m (integrated)	Moon diameter in km (in %)
45 Eugenia	2003-Dec-06 12:42	0.79	−5.3	−7.0	7 ± 1 (4%)
45 Eugenia	2003-Dec-06 14:20	0.75	−5.6	−7.4	7 ± 2 (3%)
121 Hermione	2003-Dec-06 12:30	0.19	−3.9	−5.7	13 ± 4 (7%)
121 Hermione	2003-Dec-06 14:03	0.24	−3.8	−5.7	11 ± 3 (7%)
130 Elektra	2003-Dec-07 07:16	0.79	−5.6	−7.4	6 ± 2 (3%)
107 Camilla	2004-Oct-25 06:53	0.59	−4.7	−6.1	11 ± 2 (6%)
87 Sylvia	2004-Oct-25 06:29	0.22	−2.9	−5.4	20 ± 5 (7%)

Notes. The moon diameter was directly estimated from the Δ_m (integrated). The uncertainty indicated corresponds to the 1-σ error on the measurement.

asteroids with $D < 200$ km, $D_{\rm IRAS}$ was underestimated on average by 6–8%.

4.1. Comparison of AO images with lightcurve inversion models

Several asteroids in this paper have been analyzed via lightcurve inversions by Kaasalainen et al. (2002b), Michałowski et al. (2004) and Torppa et al. (2003). We compared the inversion model plane-of-sky predictions with the observed images. The model was produced with the same scattering model described in the corresponding inversion articles. In many cases, the AO images approached the same level of detail as the lightcurve models, and for 9 Metis and 130 Elektra the images may even reveal some features not resolvable by photometry. Slight albedo variations are not expected to affect the global shape model significantly. This is called Minkowski stability (Kaasalainen and Torppa, 2001): it can be shown that attributing photometric variations to shape is a considerably more stable process than attributing them to albedo. Also, photometric inversion provides a measure of probable albedo variegation, which so far has been significant (though still moderate) for only a few asteroids out of about one hundred. Spacecraft images appear to corroborate this. In a future paper (Kaasalainen and Marchis, in preparation), we will simultaneously combine the complementary data sources of adaptive optics images and photometry to make shape/albedo/rotation models that produce mutually consistent plane-of-sky images and lightcurves. Such multi-data inversions considerably reduce the modeling uncertainties (Kaasalainen and Lamberg, 2006).

Comparing the AO images with 3D-models allows us to discard the photometric mirror pole solution inevitable for asteroids moving close to the plane of the ecliptic. The plane-of-sky model image for the wrong pole is usually clearly different from the AO image in orientation and also shape. Thus even limited angular resolution AO images reveal the correct pole solution. The photometric inversion models agree well with the AO images, thus confirming the validity of both the lightcurve inversion method [much as space probe ground truths in Kaasalainen et al. (2001)] and the AO image reduction technique.

4.2. 9 Metis

Fig. 6 shows the basic-processed and deconvolved unsaturated images of 9 Metis. This S-type asteroid was observed twice on October 25, 2004 at 06 UT and 2 h later. The average size of 181 km is close to the 190 km size reported by Kristensen (1984). At 650 km from the center of the primary (corresponding to $2/100 \times R_{\rm Hill}$) the minimum detectable size for a companion was 5.4 km. At $1/4 \times R_{\rm Hill}$ the detectivity improved and a 4 km moonlet would have been unambiguously detected. We did not see the companion reported by Wang et al. (1981) located at ∼1100 km with a ∼60 km diameter. Considering the excellent sensitivity in our image, such a large companion could go unseen only if the orbit is nearly edge-

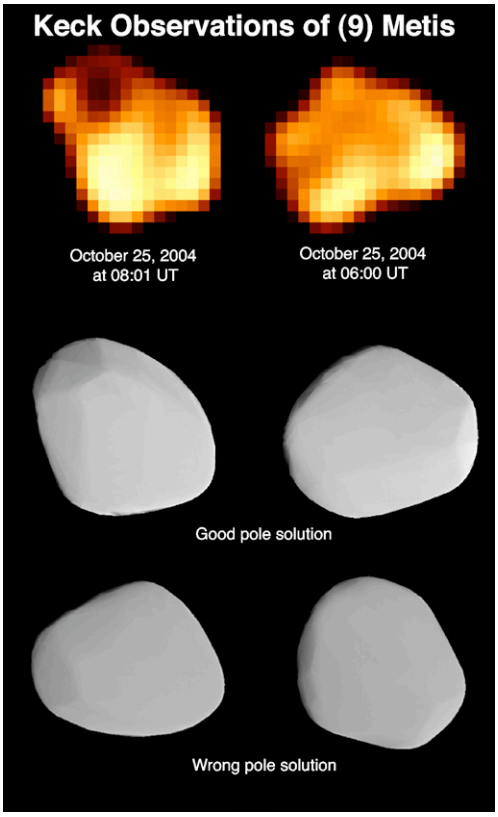

Fig. 6. 9 Metis observed with the Keck NGS AO system at 2.1 μm with a pixel scale of 9.94 mas. The AIDA deconvolved images are at the top. The asteroid is nearly seen from the pole (viewing angle of 20°). Surface markings are clearly detected on both images with contrasts up to 50%. A comparison with the apparent shape and orientation with Torppa et al. (2003) shape model, pole solution ($\lambda = 181°$, $\beta = +23°$ in ECJ2000) and known lightcurve rotational phase confirms the accuracy of their model (middle). The bottom 3D-model displayed shows Metis asteroid with the clearly wrong pole solution. Both images are separated by 142° in rotation phase.

on from Earth, and if the satellite is located in front or behind the primary. We calculated that the absence of a 60 km diameter companion around Metis is confident at 95%. The apparent size ratio (a/b) of the asteroid is 8% smaller than the one reported by lightcurve observations suggesting that we did not observe 9 Metis at its maximum apparent size. A 3D ellipsoid model proposed by Mitchell et al. (1995) by combination of radar, and lightcurve measurements indicates that 9 Metis can be approximated by an ellipsoid with $2a = 215$ km, $2b = 170$ km, and $2c = 135$ km. Fig. 6 shows a close-up view of both Metis observations. In fact, the asteroid is quite irregular in shape and displays albedo features with a contrast of up to 50%. Our simulations (Section 3.1) showed that the contrast in deconvolution artifacts for Metis-sized objects was always <15%. Hence, these surface markings are consequently real. The most prominent one corresponding to a low albedo area (contrast ∼50%) is located at the astronomical north of the 08 UT image. The bright structure in the astronomical south-west with a contrast of 20% is visible on both images. These observations were recorded using a Kp broadband filter from 1.95 to 2.30 μm. In this wavelength range, mafic minerals show a very strong absorption in their reflectance (Gaffey et al., 1993) suggesting a heterogeneous distribution of this mineral on the surface of 9 Metis. Photo-polarimetric observations by Nakayama et al. (2000) also indicates a heterogeneous surface for Metis.

The variations in intensity may not be caused by albedo markings only. The lightcurve inversion model images displayed in Fig. 6 do not have any albedo features, yet they are bright and dark in several same areas as the AO images. In fact, surface scattering properties (different viewing and illumination directions, i.e., "subsolar brightening" of a dark surface of irregular shape) also contribute to the variation of light. The relative contributions of albedo, scattering, and shape will be better quantified in Kaasalainen and Marchis (in preparation). Because of 9 Metis' irregular shape and the significant variation of brightening on its surface, it is possible that it is made up by the combination of accreted chunks. By combining this work with spectroscopic analysis, it should be possible to better characterize the surface composition.

The lightcurve pole solution of ($\lambda = 181°$, $\beta = +23°$ in ECJ2000) from Torppa et al. (2003) is clearly the correct one, demonstrating that AO can remove the pole ambiguity, and the shape solution fits the image well. This solution is also in excellent agreement with the HST image taken by Storrs et al. (1999).

4.3. 52 Europa

52 Europa, a C-type asteroid, was observed once on December 7, 2003 at 07:50 UT. Fig. 7 shows how remarkably close this asteroid is to a perfect ellipse. No moonlet companion was detected around 52 Europa; at $2/100 \times R_{\mathrm{Hill}}$, the minimum detectable moonlet size was 9.2 km. Its average measured size of 308 km is very close to the D_{IRAS} measurement of 302 km indicating that we are observing the asteroid at its maximum apparent size. The apparent shape of the asteroid can be well approximated by an ellipse with $2a = 349 \pm 2$ km and

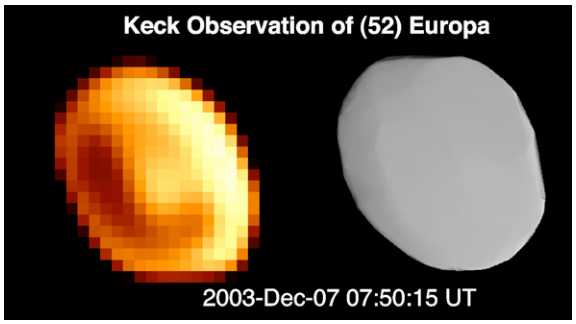

Fig. 7. Observation of 52 Europa with Keck AO system (pixel scale of 9.94 mas) (left). One dark structure with a contrast of 19% is detectable close to the north-east limb. The other structures are probably artifact of deconvolution (contrast < 12%). A comparison with the shape obtained by lightcurve inversion is display on the right. With the lightcurve pole solution ($\lambda = 252°$, $\beta = +38°$ in ECJ2000) and lightcurve rotational phase from Michałowski et al. (2004) (viewing angle of 46°) the shape is well consistent with the Keck AO image.

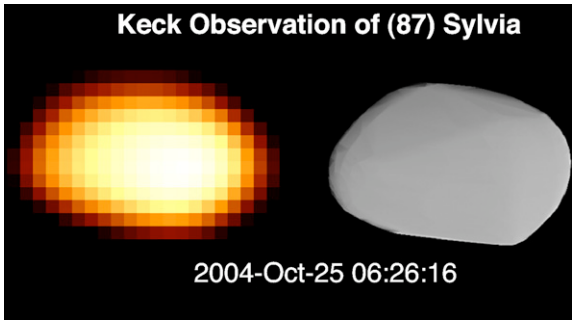

Fig. 8. Observation of 87 Sylvia with Keck AO system in K band with a pixel scale of 9.94 mas (left). No albedo markings are detectable on this 2.1 μm image. A comparison with the shape obtained by lightcurve inversion is display on the right. The pole solution ($\lambda = 72°$, $\beta = +66°$ in ECJ2000), shape and lightcurve rotational phase from Kaasalainen et al. (2002b) (viewing angle of 75°) is quite consistent with the image.

$2b = 267 \pm 1$ km leading to $a/b = 1.30 \pm 0.01$. Surface features are not well detected since no specific PSF was taken for this target. Our deconvolution with AIDA shows a typical artifact of deconvolution (bright edge and bright peak in the middle of the asteroid) with a contrast <10% (Fig. 7). One dark structure with a contrast of 19% is detectable close to the north-east limb, but it remains quite marginal and additional observations and a more careful deconvolution analysis is needed to confirm the presence of surface markings on this asteroid. Comparing 52 Europa with 9 Metis, an S-type asteroid, it is clear that they are quite different in composition and shape, which is probably due to a difference in formation and evolution.

The lightcurve pole solution of ($\lambda = 252°$, $\beta = +38°$ in ECJ2000) from Michałowski et al. (2004) is the correct one, resolving the pole ambiguity; the shape is also consistent with the image.

4.4. 87 Sylvia

87 Sylvia was observed on October 25, 2004 at 06:30 UT. Around this C-type asteroid orbits a moonlet companion dis-

covered by Brown et al. (2001). We successfully detected this companion at 0.236 arcsec (peak intensity of 2.9 magnitude), corresponding to an apparent separation of 445 km, much closer than expected for the semi-major axis reported in Merline et al. (2002). Assuming the same albedo for the primary and secondary, the integrated flux ratio of Δm(integrated) = 5.4 indicates a typically-sized companion diameter of $\sim 20 \pm 5$ km. Sylvia's primary was resolved with an average diameter ($D =$ 282 km) that was 7% larger than the IRAS radiometric diameter ($D_{\rm IRAS} = 261$ km). The primary displays an elliptical shape and does not seem to be binary as suggested by Prokof'eva and Demchik (1994) based on the light variation analysis with several optical filters. The best elliptical fit of Sylvia resulted in $2a = 348 \pm 1$ km and $2b = 217 \pm 6$ km and a ratio of $a/b = 1.60$, although lightcurve measurements suggest that $a/b \sim 1.77$. No albedo structures were detected on this hemisphere of the asteroid. The pole solution ($\lambda = 72°$, $\beta = +66°$ in ECJ2000) and shape from Kaasalainen et al. (2002b) is consistent with the image (see Fig. 8).

Marchis et al. (2005b) reported recently the discovery of a second moonlet [named (87) Sylvia II Remus] around 87 Sylvia using NACO, the adaptive optics system available on the ESO-VLT UT4 telescope. Because this satellite is closer and fainter, it is more difficult to detect on their AO observations. We carefully searched for it on the Keck observation after subtracting the azimuthally averaged profile. A secondary point-like structure appears, ~2–3 magnitude fainter (peak intensity = 6.3) can be seen at 0.349″ east of the primary, corresponding to 660 km (see Fig. 15). This detection is marginal (the 2-σ detection limit at this distance is 5.1) but compatible in position with the semi-major axis reported in Marchis et al. (2005b) ($a = 706$ km).

4.5. 130 Elektra

On December 7, 2003 at 07:16 UT we observed 130 Elektra, a G-type asteroid. This C-type sub-class is characterized by a low albedo ($A \sim 0.05$) and strong UV absorption (Tholen and Barucci, 1989). A moonlet companion orbiting around 130 Elektra was recently discovered by Merline et al. (2003). Its orbital elements, however, are mysterious (Marchis et al., 2005a) and additional are taken by our group to refine them. The satellite companion was successfully detected on our Kp band image with a Δm(integrated) = 7.4 and with an angular separation of 0.79″, corresponding to an apparent separation of 1040 km. Assuming the same surface albedo for Elektra and its moonlet, we derived a diameter for the secondary of ~6 km.

Elektra's primary shape is quite irregular as shown on our AO resolved observation displayed in Fig. 9. Its mean size ($D = 191$ km) is slightly larger than the one derived from radiometric IRAS measurements. Its surface displays several albedo features with a contrast of ~5–15%. A better characterization of 130 Elektra surface will soon be possible using AO systems combined with spectro-imager instruments.

The pole solution of ($\lambda = 68°$, $\beta = -88°$ in ECJ2000), period 5.2247 h and shape from Ďurech et al. (in preparation) agrees well with this image and again removes the pole ambiguity.

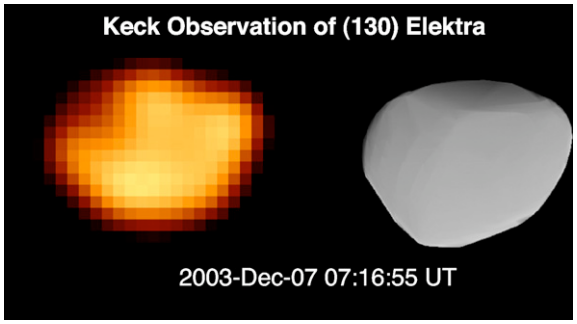

Fig. 9. Observation of 130 Elektra with Keck AO system in K band with a pixel scale of 9.94 mas (left). Elektra shape is quite irregular and several albedo features are observed at 2.1 μm. A comparison with the shape obtained by lightcurve inversion is display on the right. The pole solution ($\lambda = 68°$, $\beta = -88°$ in ECJ2000), period 5.2247 h, shape and lightcurve rotational phase from Ďurech et al. (in preparation) agrees well with the image and again removes the pole ambiguity (viewing angle of 127°).

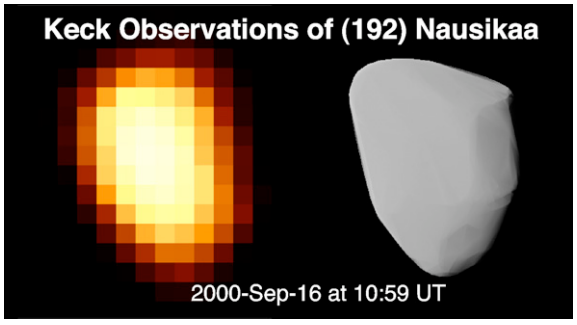

Fig. 10. Observation of 192 Nausikaa with Keck AO system in H band with KCAM IR test camera (pixel scale of 16.8 mas) (left). Nausikaa shape is quite irregular and no albedo features are observed at 1.6 μm. The lightcurve inversion shape with a new pole solution of ($\lambda = 326°$, $\beta = +33°$ in ECJ2000), sidereal period of 13.6217 h and known lightcurve rotation phase [a prograde version of the pole in Kaasalainen et al. (2002b)] displayed on the right is consistent with the AO observation (viewing angle of 111°).

4.6. 192 Nausikaa

On September 16, 2000, shortly after the final commissioning of the Keck AO system, 192 Nausikaa, an S-type asteroid, was observed by D. Le Mignant with the KCAM IR test camera. Two observations were recorded with a 16.8 mas pixel scale in the H band (1.6 μm). No moonlet companion was detected but the primary was clearly resolved with an average size of 86 km and an elliptical ratio of $a/b = 1.51$ (slightly smaller than the ratio estimated by lightcurve observations). Fig. 10 shows that this hemisphere of the asteroid surface does not display any obvious surface features at 1.6 μm.

As we later found out, a few pole solutions in Kaasalainen et al. (2002b) and Torppa et al. (2003) were offset due to an error in one of the version of the program used to read the Uppsala database (UAPC) (cf. Michałowski et al., 2004). Fortunately, this version was used only for a small part of the datasets, and the error affected only a fraction of them. 192 Nausikaa was one of the affected targets; an updated solution ($\lambda = 326°$, $\beta = +33°$ in ECJ2000) and sidereal period of 13.6217 h a prograde version of the pole in Kaasalainen et al. (2002b) is consistent with the images. The existing lightcurve set is underdeter-

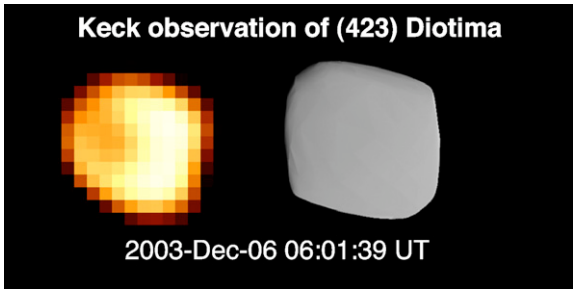

Fig. 11. Observation of 423 Diotima with Keck AO system in K band with a pixel scale of 9.94 mas (left). No albedo feature are visible on the AO image and no companion with a diameter >7.8 km (>5.9 km) orbits around Diotima primary at $2/100 \times R_{\rm Hill}$ ($1/4 \times R_{\rm Hill}$). The left image is a comparison with the Kaasalainen and Marchis (in preparation) shape model considering a pole solution ($\lambda = 353°$, $\beta = +2°$ in ECJ2000) and a period 4.77538 h (viewing angle of 161°). The apparent shape of the Keck AO and the model agree quite well removing the pole ambiguity.

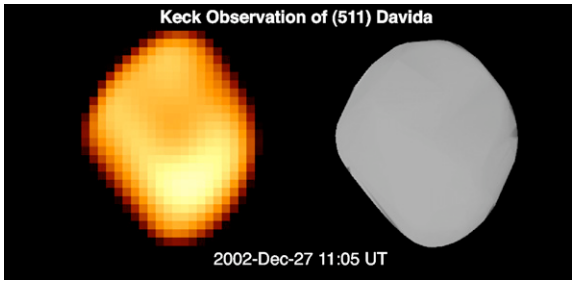

Fig. 12. Observation of 511 Davida with Keck AO system by the Keck Science team in K band (pixel scale of 9.94 mas) (left). The surface of the asteroid does not show any obvious surface markings. The left image is a comparison with Torppa et al. (2003) shape model, including an updated pole solution ($\lambda = 297°$, $\beta = +26°$ in ECJ2000), period 5.129363 h (viewing angle of 27°). The shape model derived from lightcurve measurement is in excellent agreement with the Keck AO image.

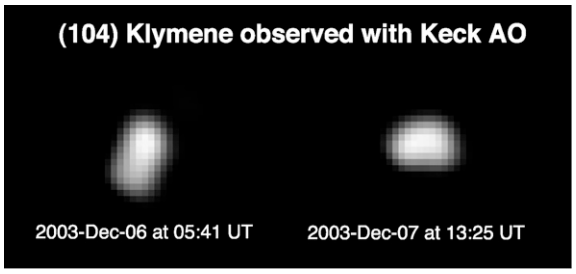

Fig. 13. Two Keck AO observations of 104 Klymene taken in December 2003 in K band with a pixel scale of 9.94 mas. A bilobated shape for this main-belt asteroid is suggested on the observation recorded on December 6, 2003, but not confirmed on December 7, 2003. The suggested apparent bifurcated shape of 104 Klymene can be approximated considering two spheres with a $R_1 = 55$ km and $R_2 = 60$ km imbricated into each other and with a separation of 70 km.

mined with only three oppositions, leading to a threefold pole degeneracy with a weak constraint on pole latitude and shape. The AO image clearly singled out the right pole (Fig. 10). The last observation epoch of the lightcurve set is from 1985, so the rotation phase of the model is apparently slightly offset from the one of the AO image.

4.7. 423 Diotima

423 Diotima, a C-type asteroid, was observed on December 6, 2003. This asteroid is the largest member of a collisional family (Karachkina and Prokofeva, 2003) and is suspected to have a satellite companion due to a lightcurve anomaly observed in 1982 by Schober (1983). With a mean angular size estimated to be 125 mas, the Keck AO system easily resolved the primary. Its estimated size is very close to the IRAS diameter measurement (208 km), probably because the asteroid shape is nearly spherical with a size ratio of $a/b = 1.08$. No albedo features were visible on the AO image and no companions with a diameter >7.8 km (>5.9 km) were seen to orbit Diotima's primary at $2/100 \times R_{\rm Hill}$ ($1/4 \times R_{\rm Hill}$) and between (see Fig. 5b for details). Fig. 11 displays a close-up of the primary and a comparison with the shape model of (Kaasalainen and Marchis, in preparation) using a pole solution of ($\lambda = 353°$, $\beta = +2°$ in ECJ2000) and a period 4.77538 h. The apparent shape of the Keck AO image and the model agree quite well, and thus remove the pole ambiguity.

4.8. 511 Davida

511 Davida is the largest asteroid observed in this survey with an average observed diameter of 316 km. We describe one set of processed observations extracted from a set of data covering a full rotation acquired by the Keck Science team (Conrad et al., 2003). Davida was observed at its maximum apparent size. The measured size and ratio a/b are slightly smaller than the IRAS average diameter and the maximum ratio determined by the lightcurve measurements. Fig. 12 shows that no obvious surface markings are visible on the Kp-band image of this hemisphere. Most of the markings shown have a contrast of <5% and may simply be artifacts of deconvolution. A more accurate analysis (e.g., tuning the regularization parameters of deconvolution) on a larger set of images involving a cross-correlation of features could be used to confirm the existence of any albedo markings.

The pole solution in Torppa et al. (2003) is offset; the updated lightcurve solution ($\lambda = 297°$, $\beta = +26°$ in ECJ2000), with a period of 5.129363 h, and shape are in an excellent agreement with the AO image.

4.9. 104 Klymene

104 Klymene intrigued us during the first observation taken on December 6, 2003. The AO image revealed a bi-lobed shape for the asteroid. A second observation taken one day later did not help to confirm this unusual shape because of the rotation of the asteroid (Fig. 13). Based on the deconvolved image, we fit the apparent shape of 104 Klymene by an ellipse with a major-axis ($2a$) of 163 ± 3 km and a minor-axis ($2b$) of 103 ± 5 km corresponding to an average size of 133 km and $a/b = 1.58$. Lightcurve measurements reported a maximum of 0.3 magnitude corresponding to a $\max(a/b)$ of 1.32. However, (104) Klymene lightcurve measurements are quite limited with a few measurements taken in September to November 1991 and analyzed by Shevchenko et al. (1992). It is possible that the asteroid was never observed at its maximum apparent size.

The apparent bifurcated shape of 104 Klymene could be approximated by two overlapping spheres with $R_1 = 55$ km and $R_2 = 60$ km and with a separation of 70 km. This shape is quite similar to the one proposed for 121 Hermione, another bi-lobed main-belt asteroid that was also observed with the Keck AO telescope (Marchis et al., 2005c). Bifurcated shapes in the near-Earth asteroid population are quite common and have been seen through radar observations [see review in Ostro et al. (2002)]. In the main-belt, the dumbbell-shape of 216 Kleopatra was accurately studied by radar (Ostro et al., 2000), AO (Hestroffer et al., 2002), and interferometric observations (Tanga et al., 2001). These exotic shapes are probably the result of collisional events. No moonlet companion with a diameter > 4.3 km (2.9 km) was seen around Klymene's primary at $2/100 \times R_{\rm Hill}$ ($1/4 \times R_{\rm Hill}$). Additional observations under excellent seeing conditions and in various filters are necessary to confirm its shape and refine the structure of 104 Klymene.

4.10. Other asteroids

The mean size and axis ratio for each asteroid is detailed in Table 5. A comparison with the radiometric IRAS diameter and the lightcurve measurements (extracted from the Minor Planet Lightcurve Parameters updated by A.W. Harris and B.D. Warner) was added.

25 Phocaea. The apparent mean size ($D = 71$ km) was consistent with an IRAS radiometric measurement ($D_{\rm IRAS} = 75$ km). A few lightcurve measurements are available for this S-type asteroid. van Houten-Groeneveld and van Houten (1958) reported a period of 9.9353 h and a minimum $\Delta m = 0.16$ corresponding to a size ratio of $a/b = 0.16$, very close to our Keck AO measurement of 0.15.

45 Eugenia. Petit–Prince, Eugenia's moonlet satellite was detected in our observations. The primary is resolved with a mean diameter of 202 km, close to the radiometric IRAS diameter of 215 km. Since our size ratio, a/b, is significantly lower than the that reported in the ephemeris, we conclude that we did not observe the asteroid at its maximum apparent size. The moonlet companion (named 45 Eugenia I Petit–Prince) located at 0.8″ has a diameter of 7 km (Fig. 15). A detailed analysis of this asteroid system based mostly on a campaign of observations performed with the VLT and Gemini AO system, a consideration of orbital elements of its secondary, and the shape of the primary is in preparation (Marchis et al., 2006).

94 Aurora. This C-type asteroid was observed only during two apparitions as reported in di Martino et al. (1987). The observed shape ratio, $a/b = 1.11 \pm 0.08$, is in agreement with their lightcurve characteristics [$\Delta m = 0.12$ ($a/b = 1.12$)]. However, the asteroid mean diameter is 20% smaller than the IRAS one.

96 Aegle. Despite several observations starting in 1980 (Harris and Young, 1989), the lightcurve of this asteroid is not well characterized. Very recently, Stephens (2005) reported a period of 13.82 h and a $\Delta m = 0.15$ ($a/b = 1.12$) from observations recorded in August 2004, very close to our Keck AO ratio of $a/b = 1.19 \pm 0.12$. The apparent mean size of 156 km is 9% smaller than the $D_{\rm IRAS}$ measurement.

102 Miriam. Two distinct Δm measurements by several groups are reported for this asteroid. Our Keck AO observed with $a/b = 1.34 \pm 0.15$ is in better agreement with the $\Delta m = 0.16$ ($a/b = 1.16$) by Harris et al. (1992) than $\Delta m = 0.08$ reported by Shevchenko et al. (1992), implying that the geometry of observations during Harris' and our observations was similar. The Keck AO mean size of 79 km is very close to the $D_{\rm IRAS} = 83$ km.

107 Camilla. The moonlet satellite of this C-type asteroid was detected in our Keck AO observation. The primary was also resolved with an average diameter of 185 km, 20% smaller than the reported $D_{\rm IRAS}$. Since our a/b is significantly smaller than the reported lightcurve a/b, we conclude that we did not observe the asteroid at its maximum apparent size. A detailed analysis of this asteroid system considering additional observations recorded with the VLT AO system, including the orbital elements of its secondary, the shape of the primary and a comparison with a shape model was recently presented (Marchis et al., 2005a). Based on our Keck observation, we estimate the moonlet to have a diameter of 11 km.

121 Hermione. Marchis et al. (2005c) present a detailed analysis of this asteroid system considering additional observations recorded with the VLT AO system, including the orbital elements of its secondary, the shape of the primary and a comparison with an ellipsoid shape model. The analysis reported here using a different deconvolution method confirms the bilobated shape of the asteroid and its apparent size. The companion of 121 Hermione, with an estimated diameter of ∼12 km is detected on two images with an angular separation of 0.2″ from the primary.

165 Loreley. Our measurement indicates a size ratio $a/b = 1.26 \pm 0.08$ slightly higher than the one derived using measurements of Harris et al. (1992) ($\Delta m = 0.12$–0.15; $a/b = 1.12$–1.15). Using multiple lightcurve observations of the asteroid, Blanco and Riccioli (1998) determined the orientation of its rotational axis and its shape using the amplitude–magnitude method suggested by Zappala (1981). They reported a pole orientation of $\lambda = 159 \pm 18$ and $\beta = -65 \pm 18$ in ECB1950 and ellipse ratios $a/b = 1.19$ and $b/c = 1.27$. Using these parameters, we generated the apparent shape and orientation on the sky of 165 Loreley at the epoch of our observations (Fig. 14). At the epoch of the observation, the apparent size ratio and orientation of Zappala (1981) are roughly in agreement with our observations with $a/b = 1.37$ (close to the measured $a/b = 1.26$) and an ellipse tilted by 20° relative to our Keck AO observation.

175 Andromache. The mean diameter derived from our Keck observation ($D = 107$ km) is close to the radiometric diameter by IRAS ($D_{\rm IRAS} = 101$ km). However, the apparent shape of

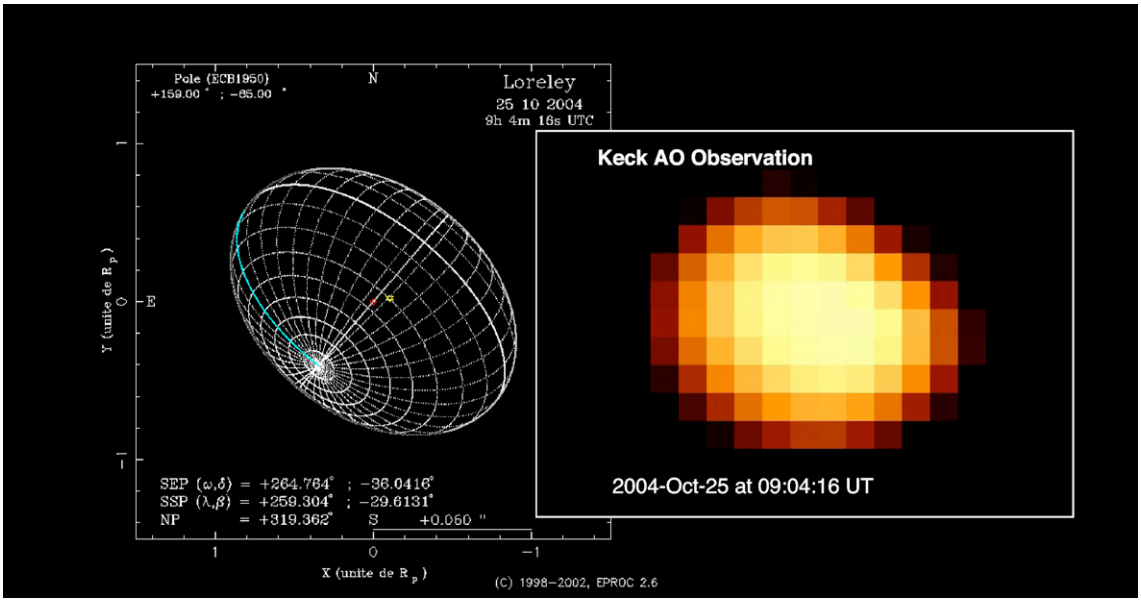

Fig. 14. Observations of 165 Loreley with Keck AO system at 2.1 μm with a pixel scale of 9.94 mas (left). The apparent shape and orientation using the pole solution of Blanco and Riccioli (1998) and ellipse shape is displayed. The measured size ratio ($a/b = 1.26 \pm 0.08$) is in agreement with the one provided by the physical ephemeris ($a/b = 1.37$). The apparent angle is slightly different, but consistent with the uncertainty of the pole solution since the ellipse is tilted by $\sim 20°$.

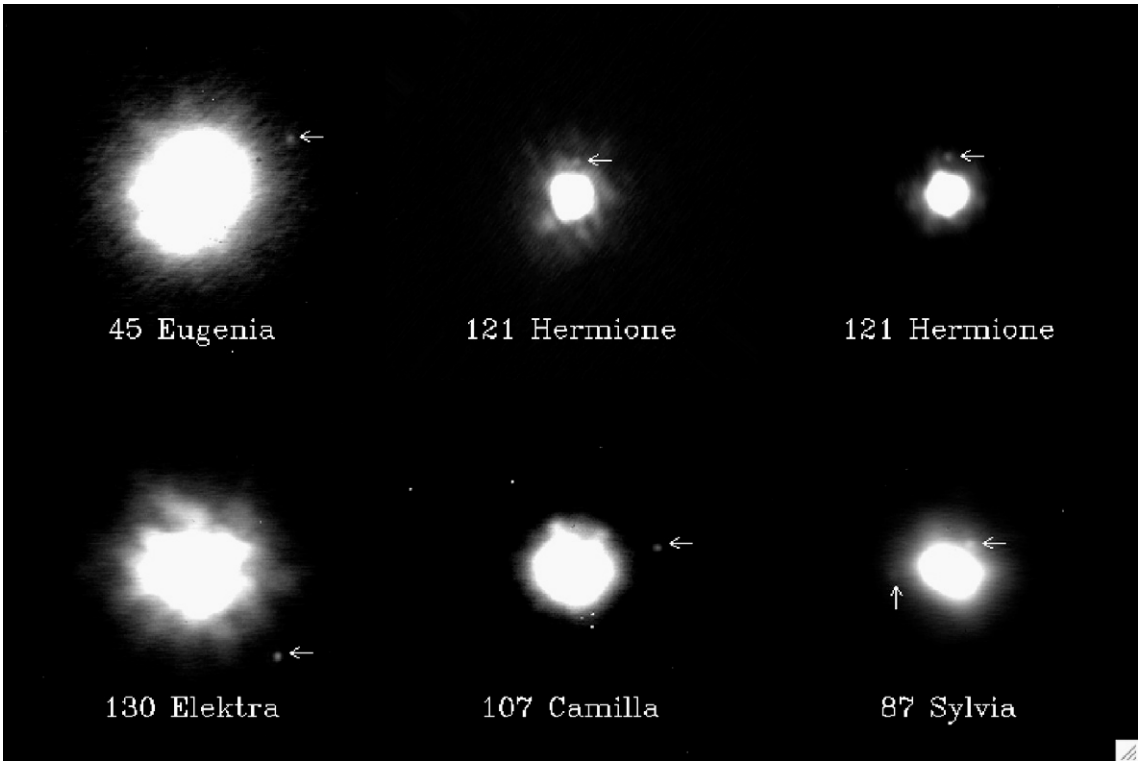

Fig. 15. Moonlet companions of 45 Eugenia [named (45) Eugenia I Petit–Prince], 121 Hermione [temporary name S/2001 (121) 1], 130 Elektra [temporary name S/2003 (130) 1], 107 Camilla [temporary name S/2003 (107) 1] and 87 Sylvia [named (87) Sylvia I Romulus] detected on our data (indicated by an horizontal arrow). The intensity is stretched to display the low level. The halo due to the imperfection of the AO phase correction can be seen surrounding the primary. Its intensity limits the detection of closer and fainter moonlets. A vertical arrow was added on 87 Sylvia image to show the possible position of the secondary moonlet [named (87) Sylvia II Remus].

the asteroid is roughly circular ($a/b = 1.09 \pm 0.09$) whereas Blanco et al. (2000) reported a $\Delta m = 0.21$, leading to a size ratio of $a/b = 1.20$. This asteroid was not observed at its maximal apparent size.

182 Elsa. This asteroid is the only one which is not resolved in this survey. With a $D_{\mathrm{IRAS}} = 45$ km and a distance of 1.09 AU, its expected angular diameter is 55 mas, very close to the angular resolution of the instrument. The size ratio measured by

lightcurve measurements (Harris et al., 1992) indicates that Elsa is very elongated ($a/b = 1.9$), and also has a very slow rotation ($P \sim 80$ h).

194 Prokne. Only one incomplete lightcurve of this C-type asteroid has been reported by Scaltriti and Zappala (1979) with a period of ~ 15.57 h and a $\Delta m = 0.27$ corresponding to a size ratio of $a/b = 1.28$. Our observation indicates an average size of 151 km, close to the 164 km IRAS radiometric diameter, but with a smaller $a/b = 1.13 \pm 0.06$. Prokne was not observed at its maximum apparent size.

198 Ampella. Two measurements with a large discrepancy are reported in the Minor Planet Lightcurve Parameters table. Deyoung and Schmidt (1993) reported on observations performed in February 1993 and derived a lightcurve with the following characteristics: $\Delta m = 0.22$ ($a/b = 1.22$) with $P = 10.38$ h. In contrast, Calabresi et al. (1996) detected a very small variation of $\sim$0.03 in maximum magnitude. Even though this asteroid's angular size ($\sim$70 mas) is close to the angular resolution of the telescope, it was clearly resolved by our Keck AO observation. Its average size ($D = 53$ km) and its measured size ratio ($a/b = 1.22$) is in agreement with the IRAS diameter (57 km) and the lightcurve size ratio of Deyoung and Schmidt (1993).

259 Aletheia. The lightcurve of this asteroid remains unknown. Weidenschilling et al. (1990) reported a minimal period of 15 h with a $\Delta m \sim 0.1$. Unpublished results by Robinson (personal communication, 1993) suggest a period of 12.2 h with an amplitude of 0.19 magnitude ($a/b = 1.19$). We derived a size ratio ($a/b = 1.21$) very close to the latter measurement, though with a relatively significant error bar for the measurement. The observed diameter was 6% larger than the IRAS average diameter ($D = 190$ km).

264 Libussa. With a mean angular diameter of 57 mas, this asteroid is very close to the limit of resolution for our observations. The image clearly displays an asymmetrical shape for the asteroid. A fit of the deconvolved image yields a minor axis of $2b = 42$ mas, which is the theoretical resolution of the telescope at 2.1 μm. We cannot conclude much about this asteroid except that it is resolved only in the direction of its major axis $2a = 66 \pm 7$ km. Its size ratio as estimated by lightcurve measurements indicate that the amplitude is larger than 0.22 in magnitude, corresponding to $a/b > 1.22$.

308 Polyxo. This U-type asteroid's lightcurve characteristics are well-defined, with $P = 12.03$ and a $\Delta m = 0.20$ ($a/b = 1.20$) (Harris and Young, 1983). The apparent shape on the Keck AO image ($a/b = 1.26 \pm 0.11$) is in agreement with this lightcurve size ratio. The average diameter ($D = 130$ km) is 8% smaller than the radiometric IRAS one.

385 Ilmatar. Because the shape ($D = 69$ km) and the size ratio ($a/b = 1.30 \pm 0.30$) measured on the Keck AO image are significantly smaller than the IRAS diameter ($D_{\mathrm{IRAS}} = 91$ km) and the lightcurve size ratio [$a/b = 1.58$ from Worman et al. (2004)], we conclude that this asteroid was not observed at its maximum apparent size on December 6, 2003.

444 Gyptis. The average size diameter measured in our survey ($D = 129$ km) for this C-type asteroid was significantly smaller than the IRAS diameter ($D = 160$ km). Additionally, the apparent size ratio of $a/b = 1.40$ was larger than one derived by a lightcurve measurement of Harris et al. (1984). Gyptis was well resolved with an apparent mean angular size of 90 mas, so we are confident that our analysis is accurate. The significant variations in estimated diameters indicate that Gyptis is an irregular shaped asteroid.

490 Veritas. The average diameter measured on our Keck observation ($D = 131$ km) is 12% larger than the reported IRAS diameter. Veritas' observed size ratio ($a/b = 1.29 \pm 0.11$) is slightly smaller, but within error of one derived by lightcurve measurements ($a/b = 1.36$) (Koff and Brincat, 2001).

654 Zelinda. With an apparent average size ($D = 131$ km) 13% smaller than the IRAS diameter, this C-type asteroid was roughly circular. However, Fig. 4 suggests that its shape is triangular. The observed size ratio ($a/b = 1.0$) is much smaller than the size ratio of 1.32 reported Schober (1975) through lightcurve measurement. Once again we did not observe this asteroid at its maximum apparent size.

674 Rachele. Several observations of this S-type asteroid were recorded on December 7, 2003 because a moonlet companion appeared to be orbiting $0.17''$ away from the primary in the first observation. After recording several PSF frames and one additional observation of Rachele a few hours later, we concluded that it was an artifact of the Keck AO. The average diameter of the asteroid measured on our data ($D = 89$ km) and the size ratio ($a/b = 1.08$) is in agreement with the IRAS diameter ($D = 97$ km) and the lightcurve measurement ($a/b = 1.15$) from Harris et al. (1992).

679 Pax. With an apparent size ratio of $a/b = 1.66 \pm 0.23$, this asteroid is one of the most elongated in our survey. Its mean size ($D = 62$ km) is 16% larger than the IRAS one. Several lightcurve observations are available; Schober et al. (1994) report a much larger $\Delta m = 0.3$ ($a/b = 1.34$ with a $P = 8.452$ h) during observations performed in September 1982. The geometrical view in our observations in December 2003 are similar to those of September 1982. A more accurate analysis of the lightcurve measurements combined with our AO observations should allow us to develop an accurate shape model for this asteroid.

702 Alauda. The mean apparent size ($D = 175$ km) of this large C-type asteroid is 11% smaller than the one derived with IRAS measurement. di Martino et al. (1987) reports a $P = 8.36$ h and $\Delta m = 0.11$ ($a/b = 1.11$) in agreement with our $a/b = 1.08$.

804 Hispania. The mean apparent size ($D = 122$ km) of this C-type asteroid is 30% smaller than the IRAS one. Several lightcurve measurements (see Pray, 2004 and references therein) indicate a $\Delta m \sim 0.20$, corresponding to a size ratio of $a/b = 1.25$ that is close to the one estimated from our Keck observation ($a/b \sim 1.16$).

914 Palisana. The apparent size ($D = 76$ km) and the size ratio ($a/b = 1.16$) of our Keck AO observation is in agreement with the IRAS measured diameter and the size ratio derived from lightcurve observations (Riccioli et al., 1995).

980 Anacostia. The apparent size of this S-type asteroid ($D = 70$ km) is 23% smaller than the IRAS radiometric measurement. The observed size ratio ($a/b \sim 1.09$), however, is in agreement with one estimated by lightcurve measurements ($a/b = 1.10$) (Harris and Young, 1989). Nevertheless, our measurement is quite reliable: the angular diameter of the asteroid is ∼75 mas, corresponding to an uncertainty of 6 km on the major axes of Anascotia.

5. Conclusion

We reported 41 observations of 33 individual main-belt asteroids with a diameter >40 km taken with the Keck AO system mostly in 2003 and 2004, with additional observations of 192 Nausikaa in September 2000 and 511 Davida in December 2002. Five of them (45 Eugenia, 87 Sylvia, 107 Camilla, 121 Hermione, 130 Elektra) were already known to have a secondary moonlets whose existence was confirmed by our Keck AO survey. The size of these moonlets, assuming the same albedo as the primary moon is small, ∼5% the size of their primary counterpart (180–260 km) and suggests that they are fragments captured after a disruptive collision of a parent body (Durda, 1996; Doressoundiram et al., 1997) or a fragment ejected after collision.

For all observations in our survey, a 2-σ detection curve was calculated and synthesized by an approximation of two linear functions characterized by three parameters. The minimum size of a moonlet as a function of distance from the primary in $R_{\rm Hill}$ was determined for each asteroid. Most of the known binary asteroids have a companion satellite orbiting well inside the Hill sphere at $\sim 2/100 \times R_{\rm Hill}$. However, since 749 Balam and 379 Huenna are two binary systems characterized by a loosely-bound companion located at $1/4 \times R_{\rm Hill}$ and $1/8 \times R_{\rm Hill}$, respectively, we searched for any additional, or distantly, orbiting satellite. Our measurements show that we should have detected new moonlet asteroids at $2/100 \times R_{\rm Hill}$ ($1/4 \times R_{\rm Hill}$) with diameters larger than 6 km (4 km). The ratio of binary asteroids in this survey was quite high (∼15%), though probably biased by selecting the previously identified binary systems in the list of 120 available targets observable each night. Given that ∼120 targets are observable each night, our survey suggests that the percentage of binary asteroids with $D > 40$ km is at less than ∼4%.

The existence of triple and multiple systems have been suggested by Doressoundiram et al. (1997) and Durda (1996). None of these were detected in our survey, however even though our measurement sensitivity of $1/4 \times R_{\rm Hill}$ would have allowed us to detect fragments up to ∼50 times smaller than the primary asteroid. We did not observe remnants of swarm fragments predicted by simulations of Michel et al. (2001) and Durda et al. (2003) after disruption of the parent asteroid. It is possible, as suggested by Merline et al. (2002), that the time-scale of these simulations was too short to examine the long term stability of such small multiple moonlets. The secondary moonlet of 87 Sylvia, discovered by Marchis et al. (2005b), was barely detected in this data set since its intensity was below the limit of detection, due to poor quality of this observation.

The apparent size and shape of each asteroid were estimated after deconvolution using a new algorithm, called AIDA developed by Hom et al. (2006). Their shape and orientation were determined by fitting the resulting deconvolved image by an ellipse. For most asteroids, their mean size was in good agreement with the IRAS radiometric measurement, even though the diameters for asteroids with $D < 200$ km were typically underestimated by 6–8%. For two asteroids, 804 Hispania and 980 Anascotia, their observed mean size was ∼20% smaller than the diameter reported by Tedesco et al. (2002). 679 Pax is 16% larger than its IRAS diameter. Nevertheless, the size a/b ratios for these asteroids were in very close agreement with those derived from lightcurve measurements in the literature (reported in the Minor Planet Lightcurve Parameters[4] updated by A.W. Harris and B.D. Warner).

One observation of 104 Klymene suggests a bifurcated shape for this asteroid. The bi-lobed structure of 121 Hermione observed by Marchis et al. (2005c) was confirmed in this study. The proportion of contact binaries in our survey which is limited to asteroids larger than 40 km is surprisingly high (∼6%). Such contact binaries are known to be quite common among near-Earth asteroids (Bottke and Melosh, 1996) as observed by radar (Hudson and Ostro, 1994). More recently, the bifurcated shape of 216 Kleopatra main-belt asteroid was confirmed nearly simultaneously by radar observation (Ostro et al., 2000) and using adaptive optics (Marchis et al., 1999; Hestroffer et al., 2002) on the ESO 3.6-m-telescope. Lightcurve inversion also revealed the binary structure of large main-belt asteroids (Kaasalainen et al., 2002a) such as 44 Nysa and 41 Daphne. These findings suggest that a non-single configuration should be common in the main-belt as well.

9 Metis, 52 Europa, 87 Sylvia, 130 Elektra, 192 Nausikaa, 423 Diotima, and 511 Davida were analyzed with lightcurve inversion (Kaasalainen et al., 2002b; Kaasalainen and Marchis, in preparation; Michałowski et al., 2004; Torppa et al., 2003). We compared the inversion model plane-of-sky predictions with the observed images. The deconvolved AO images approach the level of detail of the lightcurve model. Images of 9 Metis (S-type) and 130 Elektra (G-type) suggest some well contrasted features not resolvable by integrated photometry. The AO images also allowed us to remove the ambiguity of photometric mirror pole solution inevitable for asteroids moving close to the

[4] http://cfa-www.harvard.edu/iau/lists/LightcurveDat.html.

plane of the ecliptic (192 Nausikaa and 52 Europa). The photometric inversion models agree well with the deconvolved AO images, thus confirming the validity of both the lightcurve inversion method and the AO image reduction technique.

The use of Adaptive Optics to search for multiplicity in asteroid populations should increase with the arrival of Laser Guide Star (LGS) technology that allows astronomers to observe almost any area of the sky with a resolution close to the diffraction limit of the telescope. Fainter asteroids, such as Jupiter Trojans (Marchis et al., 2006), will be observable using these systems now available at Keck (Wizinowich et al., 2006) and VLT. Newly commissioned integral-field imagers (OSIRIS on Keck, and SPIFFI on VLT) with capabilities to record resolved spectra ($R \sim 1000$–4000) in the near-infrared (0.9–2.5 μm) will make possible to better characterize the surface mineralogy of an asteroid. A spectroscopic comparison between the primary asteroid and its moonlet will help in elucidating the origins of a system. To date, C-type asteroids have been mostly featureless in the NIR wavelength region, although weak, identifiable absorption features can be detected using state-of-the-art instrumentation (Hardersen et al., 2005). Hence, previously featureless asteroid spectra warrant re-observation with sufficiently sensitive instrumentation and angular resolution.

Acknowledgments

This work was supported by the National Science Foundation Science and Technology Center for Adaptive Optics, and managed by the University of California at Santa Cruz under cooperative agreement No. AST-9876783. These data were obtained at the W.M. Keck observatory, which is operated as a scientific partnership between the California Institute of Technology, the University of California and the National Aeronautics and Space Administration. The Observatory and its AO system were made possible by the generous financial support of the W.M. Keck Foundation. The authors wish to recognize and acknowledge the very significant cultural role and reverence that the summit of Mauna Kea has always had within the indigenous Hawaiian community. We are most fortunate to have the opportunity to conduct observations from this mountain.

References

Belton, M.J.S., Chapman, C.R., Veverka, J., Klaasen, K.P., Harch, A., Greeley, R., Greenberg, R., Head, J.W., McEwen, A., Morrison, D., Thomas, P.C., Davies, M.E., Carr, M.H., Neukum, G., Fanale, F.P., Davis, D.R., Anger, C., Gierasch, P.J., Ingersoll, A.P., Pilcher, C.B., 1994. First images of Asteroid 243 Ida. Science 265, 1543–1547.

Birlan, M., 2002. Dynamic and physical considerations on the asteroids density. Earth Moon Planets 88, 1–10.

Blanco, C., Riccioli, D., 1998. Pole coordinates and shape of 30 asteroids. Astron. Astrophys. Suppl. Ser. 131, 385–394.

Blanco, C., Di Martino, M., Riccioli, D., 2000. New rotational periods of 18 asteroids. Planet. Space Sci. 48, 271–284.

Bottke, W.F., Melosh, H.J., 1996. Binary asteroids and the formation of doublet craters. Icarus 124, 372–391.

Britt, D.T., Yeomans, D., Housen, K., Consolmagno, G., 2002. Asteroid density, porosity, and structure. In: Bottke Jr., W.F., Cellino, A., Paolicchi, P., Binzel, R.P. (Eds.), Asteroids III. Univ. of Arizona Press, Tucson, pp. 485–500.

Brown, M.E., Margot, J.L., de Pater, I., Roe, H., 2001. S/2001 (87) 1. IAU Circ. 7588.

Calabresi, M., Panella, M., Pelloni, A., 1996. Photoelectric photometry of the Asteroid 198 Ampella. Minor Planet Bull. 23, 29.

Conrad, A., Le Mignant, D., Dumas, C., Merline, W.J., Hammel, H.B., Fusco, T., Campbell, R., Chaffee, F., Goodrich, S. Kwok, R., 2003. Near-infrared imaging of large main-belt asteroids with the Keck Adaptive Optics system. AAS/Division for Planetary Sciences Meeting Abstracts 35.

Descamps, P., Marchis, F., Michalowski, T., Berthier, J., Hestroffer, D., Vachier, F., Colas, F., Birlan, M., Vieira Martins, R., 2005. Insights on 90 Antiope double asteroid combining VLT-AO and lightcurve observations. In: Asteroids, Comets, and Meteors Conference, Buzios, Brazil. Abstract.

Devillard, N., 1997. The eclipse software. The Messenger 87, 19–20.

Deyoung, J.A., Schmidt, R.E., 1993. The lightcurve and period of the S type minor Planet 198 Ampella. Minor Planet Bull. 20, 31.

di Martino, M., Zappala, V., de Sanctis, G., Cacciatori, S., 1987. Photoelectric photometry of 17 Asteroids. Icarus 69, 338–353.

Doressoundiram, A., Paolicchi, P., Verlicchi, A., Cellino, A., 1997. Formation of binary asteroids as outcomes of catastrophic collisions. Planet. Space Sci. 45, 757–770.

Dunham, D.W., Dunham, J.B., Binzel, R.P., Evans, D.S., Freuh, M., Henry, G.W., A'Hearn, M.F., Schnurr, R.G., Betts, R., Haynes, H., Orcutt, R., Bowell, E., Wasserman, L.H., Nye, R.A., Giclas, H.L., Chapman, C.R., Dietz, R.D., Moncivais, C., Douglass, W.T., Parker, D.C., Beish, J.D., Martin, J.O., Monger, D.R., Hubbard, W.B., Reitsema, H.J., Klemola, A.R., Lee, P.D., McNamara, B.R., Maley, P.D., Manly, P., Markworth, N.L., Nolthenius, R., Oswalt, T.D., Smith, J.A., Strother, E.F., Povenmire, H.R., Purrington, R.D., Trenary, C., Schneider, G.H., Schuster, W.J., Moreno, M.A., Guichard, J., Sanchez, G.R., Taylor, G.E., Upgren, A.R., von Flandern, T.C., 1990. The size and shape of (2) Pallas from the 1983 occultation of 1 Vulpeculae. Astron. J. 99, 1636–1662.

Ďurech, J., Kaasalainen, M., 2003. Photometric signatures of highly nonconvex and binary asteroids. Astron. Astrophys. 404, 709–714.

Durda, D.D., 1996. The formation of asteroidal satellites in catastrophic collisions. Icarus 120, 212–219.

Durda, D.D., Bottke, W.F., Enke, B.L., Asphaug, E., Richardson, D.C., Leinhardt, Z.M., 2003. The formation of asteroid satellites in catastrophic impacts: Results from numerical simulations. Lunar Planet. Sci. XXXIV. Abstract 1943.

Duxbury, T.C., Newburn, R.L., Acton, C.H., Carranza, E., McElrath, T.P., Ryan, R.E., Synnott, S.P., You, T.H., Brownlee, D.E., Cheuvront, A.R., Adams, W.R., Toro-Allen, S.L., Freund, S., Gilliland, K.V., Irish, K.J., Love, C.R., McAllister, J.G., Mumaw, S.J., Oliver, T.H., Perkins, D.E., 2004. Asteroid 5535 Annefrank size, shape, and orientation: Stardust first results. J. Geophys. Res. Planets 109 (E18), 2002.

Erikson, A., Berthier, J., Denchev, P., Harris, A., Ioannou, Z., Kryszczynska, A., Lagerkvist, C., Magnusson, P., Michalowski, T., Nathues, A., Piironen, J., Pravec, P., Sarounová, L., Velichko, F., 1999. Photometric observations and modeling of the Asteroid 85 Io in conjunction with data from an occultation event during the 1995–96 apparition. Planet. Space Sci. 47, 327–330.

Farinella, P., Paolicchi, P., Tedesco, E.F., Zappalà, V., 1981. Triaxial equilibrium ellipsoids among the asteroids. Icarus 46, 114–123.

Farinella, P., Paolicchi, P., Zappalà, V., 1982. The asteroids as outcomes of catastrophic collisions. Icarus 52, 409–433.

Fernández, Y.R., Sheppard, S.S., Jewitt, D.C., 2003. The albedo distribution of jovian trojan asteroids. Astron. J. 126, 1563–1574.

Fujiwara, A., Kawaguchi, J., Uesugi, K., Yeomans, D., Saito, J., Abe, M., Mukai, T., Kato, M., Okada, T., Yoshikawa, M., Yano, H., Demura, H., Scheers, D., Gaskel, R., Barnouin-Jha, O.S., Cheng, A.F., Miyamoto, H., Hirata, N., Nakamura, R., Sasaki, S., Nakamura, A.M., 2006. Global properties of 25143 Itokawa observed by Hayabusa. Lunar Planet. Sci. 37. Abstract 1575.

Gaffey, M.J., Bell, J.F., Cruikshank, D.P., 1989. Reflectance spectroscopy and asteroid surface mineralogy. In: Binzel, R.P., Gehrels, T., Matthews, M.S. (Eds.), Asteroids II. Univ. of Arizona Press, Tucson, pp. 98–127.

Gaffey, M.J., Burbine, T.H., Binzel, R.P., 1993. Asteroid spectroscopy—Progress and perspectives. Meteoritics 28, 161–187.

Hardersen, P.S., Gaffey, M.J., Abell, P.A., 2005. Near-IR spectral evidence for the presence of iron-poor orthopyroxenes on the surfaces of six M-type asteroids. Icarus 175, 141–158.

Harris, A.W., Young, J.W., 1983. Asteroid rotation IV. Icarus 54, 59–109.

Harris, A.W., Young, J.W., 1989. Asteroid lightcurve observations from 1979–1981. Icarus 81, 314–364.

Harris, A.W., Young, J.W., Dockweiler, T., Gibson, J., Poutanen, M., Bowell, E., 1992. Asteroid lightcurve observations from 1981. Icarus 95, 115–147.

Harris, A.W., Young, J.W., Scaltriti, F., Zappala, V., 1984. Lightcurves and phase relations of the Asteroids 82 Alkmene and 444 Gyptis. Icarus 57, 251–258.

Hestroffer, D., Marchis, F., Fusco, T., Berthier, J., 2002. Adaptive optics observations of Asteroid (216) Kleopatra. Astron. Astrophys. 394, 339–343.

Hom, E.F.Y., Marchis, F., Lee, T.K., Haase, S., Agard, D.A., Sedat, J.W., 2006. An adaptive image deconvolution algorithm (AIDA) with application to multi-frame and 3D data. J. Opt. Soc. Am. Submitted for publication.

Hudson, R.S., Ostro, S.J., 1994. Shape of Asteroid 4769 Castalia (1989 pb) from inversion of radar images. Science 263, 940–943.

Kaasalainen, M., Lamberg, L., 2006. Inverse problems of generalized projection operators. Inverse Probl. 22, 749–769.

Kaasalainen, M., Torppa, J., 2001. Optimization methods for asteroid lightcurve inversion. Icarus 153, 24–36.

Kaasalainen, M., Pravec, P., Krugly, Y.N., Šarounová, L., Torppa, J., Virtanen, J., Kaasalainen, S., Erikson, A., Nathues, A., Ďurech, J., Wolf, M., Lagerros, J.S.V., Lindgren, M., Lagerkvist, C., Koff, R., Davies, J., Mann, R., Kušnirák, P., Gaftonyuk, N.M., Shevchenko, V.G., Chiorny, V.G., Belskaya, I.N., 2004. Photometry and models of eight near-Earth asteroids. Icarus 167, 178–196.

Kaasalainen, M., Torppa, J., Muinonen, K., 2001. Optimization methods for asteroid lightcurve inversion. II. The complete inverse problem. Icarus 153, 37–51.

Kaasalainen, M., Torppa, J., Piironen, J., 2002a. Binary structures among large asteroids. Astron. Astrophys. 383, L19–L22.

Kaasalainen, M., Torppa, J., Piironen, J., 2002b. Models of twenty asteroids from photometric data. Icarus 159, 369–395.

Karachkina, L.G., Prokofeva, V.V., 2003. On the family of the binary Asteroid 423 Diotima. Solar Syst. Res. 37, 414–420.

Koff, R.A., Brincat, S.M., 2001. Lightcurve photometry of Asteroid 490 Veritas. Minor Planet Bull. 28, 67.

Kristensen, L.K., 1984. (9) Metis okkultationen den 19 Februar 1984. Astron. Rumfart, 76–78.

Marchis, F., Hestroffer, D., Cellino, A., Tanga, P., Zappalà, V., 1999. (216) Kleopatra. IAU Circ. 7308.

Marchis, F., Descamps, P., Berthier, J., Hestroffer, D., de Pater, I., Conrad, A., Le Mignant, D., Chaffee, F., Gavel, D., 2003a. Searching and studying binary asteroids with AO systems. AAS/Division for Planetary Sciences Meeting. Abstracts 35.

Marchis, F., Descamps, P., Hestroffer, D., Berthier, J., Vachier, F., Boccaletti, A., de Pater, I., Gavel, D., 2003b. A three-dimensional solution for the orbit of the asteroidal satellite of 22 Kalliope. Icarus 165, 112–120.

Marchis, F., Berthier, J., Descamps, P., Hestroffer, D., Vachier, F., Laver, C., de Pater, I., Gavel, D.T., 2004a. Studying binary asteroids with NGS and LGS AO systems. In: Calia, D.B., Ellerbroek, B.L., Ragazzoni, R. (Eds.), Advancements in Adaptive Optics. In: Proc. SPIE, vol. 5490. SPIE, Bellingham, WA, pp. 338–350.

Marchis, F., Descamps, P., Hestroffer, D., Berthier, J., de Pater, I., 2004b. Fine analysis of 121 Hermione, 45 Eugenia, and 90 Antiope binary asteroid systems with AO observations. AAS/Division for Planetary Sciences Meeting. Abstracts 36.

Marchis, F., Berthier, J., Clergeon, C., Descamps, P., Hestroffer, D., de Pater, I., Vachier, F., 2005a. On the diversity of binary asteroid orbits. In: Asteroids, Comets, and Meteors Conference, Buzios, Brazil. Abstract.

Marchis, F., Descamps, P., Hestroffer, D., Berthier, J., 2005b. Discovery of the triple asteroidal system 87 Sylvia. Nature 436, 822–824.

Marchis, F., Hestroffer, D., Descamps, P., Berthier, J., Laver, C., de Pater, I., 2005c. Mass and density of Asteroid 121 Hermione from an analysis of its companion orbit. Icarus 178, 450–464.

Marchis, F., Hestroffer, D., Descamps, P., Berthier, J., Bouchez, A.H., Campbell, R.D., Chin, J.C.Y., van Dam, M.A., Hartman, S.K., Johansson, E.M., Lafon, R.E., Le Mignant, D., de Pater, I., Stomski, P.J., Summers, D.M., Vachier, F., Wizinovich, P.L., Wong, M.H., 2006. A low density of 08 g cm^{-3} for the trojan binary Asteroid 617 Patroclus. Nature 439, 565–567.

Margot, J., 2002. Astronomy: Worlds of mutual motion. Nature 416, 694–695.

Merline, W.J., Close, L.M., Dumas, C., Chapman, C.R., Roddier, F., Menard, F., Slater, D.C., Duvert, G., Shelton, C., Morgan, T., 1999. Discovery of a moon orbiting the Asteroid 45 Eugenia. Nature 401, 565–567.

Merline, W.J., Weidenschilling, S.J., Durda, D., Margot, J.-L., Pravec, P., Storrs, A.D., 2002. Asteroids *do* have satellites. In: Bottke Jr., W.F., Cellino, A., Paolicchi, P., Binzel, R.P. (Eds.), Asteroids III. Univ. of Arizona Press, Tucson, pp. 289–312.

Merline, W.J., Tamblyn, P.M., Dumas, C., Close, L.M., Chapman, C.R., Menard, F., 2003. S/2003 (130) 1. IAU Circ. 8183, 1.

Michałowski, T., Kwiatkowski, T., Kaasalainen, M., Pych, W., Kryszczyńska, A., Dybczyński, P.A., Velichko, F.P., Erikson, A., Denchev, P., Fauvaud, S., Szabó, G.M., 2004. Photometry and models of selected main belt asteroids. I. 52 Europa, 115 Thyra, and 382 Dodona. Astron. Astrophys. 416, 353–366.

Michel, P., Benz, W., Tanga, P., Richardson, D.C., 2001. Collisions and gravitational reaccumulation: Forming asteroid families and satellites. Science 294, 1696–1700.

Mitchell, D.L., Ostro, S.J., Rosema, K.D., Hudson, R.S., Campbell, D.B., Chandler, J.F., Shapiro, I.I., 1995. Radar observations of Asteroids 7 Iris, 9 Metis, 12 Victoria, 216 Kleopatra, and 654 Zelinda. Icarus 118, 105–131.

Mugnier, L.M., Fusco, T., Conan, J., 2004. MISTRAL: A myopic edge-preserving image restoration method, with application to astronomical adaptive-optics-corrected long-exposure images. Opt. Soc. Am. J. A 21, 1841–1854.

Nakayama, H., Fujii, Y., Ishiguro, M., Nakamura, R., Yokogawa, S., Yoshida, F., Mukai, T., 2000. Observations of polarization and brightness variations with the rotation for Asteroids 9 Metis, 52 Europa, and 1036 Ganymed. Icarus 146, 220–231.

Ostro, S.J., Hudson, R.S., Nolan, M.C., Margot, J.-L., Scheeres, D.J., Campbell, D.B., Magri, C., Giorgini, J.D., Yeomans, D.K., 2000. Radar observations of Asteroid 216 Kleopatra. Science 288, 836–839.

Ostro, S.J., Hudson, R.S., Benner, L.A.M., Giorgini, J.D., Magri, C., Margot, J.L., Nolan, M.C., 2002. Asteroid radar astronomy. In: Bottke, W.F., Paolicchi, P., Binzel, R.P., Cellino, A. (Eds.), Asteroids III. Univ. of Arizona Press, Tucson, pp. 151–168.

Perrin, M.D., Sivaramakrishnan, A., Makidon, R.B., Oppenheimer, B.R., Graham, J.R., 2003. The structure of high Strehl ratio point-spread functions. Astrophys. J. 596, 702–712.

Pray, D.P., 2004. Lightcurve analysis of Asteroids 110, 196, 776, 804, and 1825. Minor Planet Bull. 31, 34–36.

Prokof'eva, V.V., Demchik, M.I., 1994. Fourier analysis of simultaneous BVR observations of the Asteroid 87 Sylvia and its duplicity. Astron. Lett. 20, 245–252.

Riccioli, D., Blanco, C., di Martino, M., de Sanctis, G., 1995. Lightcurves and rotational periods of main belt asteroids. III. Astron. Astrophys. Suppl. Ser. 111, 297–303.

Scaltriti, F., Zappala, V., 1979. Photoelectric photometry and rotation periods of the Asteroids 26 Proserpina, 194 Prokne, 287 Nephthys, and 554 Peraga. Icarus 39, 124–130.

Schober, H.J., 1975. The minor Planet 654 Zelinda—Rotation period and light curve. Astron. Astrophys. 44, 85–89.

Schober, H.J., 1983. The large C-type Asteroid 423 Diotima—Rotation period, lightcurve and implications for a possible satellite. Astron. Astrophys. 127, 301–303.

Schober, H.J., Erikson, A., Hahn, G., Lagerkvist, C.-I., Albrecht, R., Ornig, W., Schroll, A., Stadler, M., 1994. Physical studies of asteroids. XXVIII. Lightcurves and photoelectric photometry of Asteroids 2, 14, 51, 105, 181, 238, 258, 369, 377, 416, 487, 626, 679, 1048 and 2183. Astron. Astrophys. Suppl. Ser. 105, 281–300.

Shatsky, N., Tokovinin, A., 2002. The mass ratio distribution of B-type visual binaries in the Sco OB2 association. Astron. Astrophys. 382, 92–103.

Sheppard, S.S., Jewitt, D., 2004. Extreme Kuiper Belt Object 2001 QG298 and the fraction of contact binaries. Astron. J. 127, 3023–3033.

Shevchenko, V.G., Chernyi, V.G., Kruglyi, I.N., Lupishko, D.F., Mokhamed, R.A., Velichko, F.P., Michalowski, T., Avramchuk, V.V., Dovgopol, A.N., 1992. Photometry of seventeen asteroids. Icarus 100, 295–306.

Starck, J.L., Pantin, E., Murtagh, F., 2002. Deconvolution in astronomy. A review. Publ. Astron. Soc. Pacific 114, 1051–1069.

Stephens, R.D., 2005. Rotational periods of 96 Aegle, 386 Siegena, 390 Alma, 544 Jetta, 2771 Polzunov, and (5917) 1991 NG. Minor Planet Bull. 32, 2–3.

Storrs, A., Weiss, B., Zellner, B., Burleson, W., Sichitiu, R., Wells, E., Kowal, C., Tholen, D., 1999. Imaging observations of asteroids with Hubble Space Telescope. Icarus 137, 260–268.

Tanga, P., Hestroffer, D., Berthier, J., Cellino, A., Lattanzi, M.G., di Martino, M., Zappalà, V., 2001. NOTE: HST/FGS observations of the Asteroid (216) Kleopatra. Icarus 153, 451–454.

Tedesco, E.F., Noah, P.V., Noah, M., Price, S.D., 2002. The supplemental IRAS minor planet survey. Astron. J. 123, 1056–1085.

Tholen, D.J., Barucci, M.A., 1989. Asteroid taxonomy. In: Binzel, R.P., Gehrels, T., Matthews, M.S. (Eds.), Asteroids II. Univ. of Arizona Press, Tucson, pp. 298–315.

Thomas, P.C., Veverka, J., Simonelli, D., Helfenstein, P., Carcich, B., Belton, M.J.S., Davies, M.E., Chapman, C., 1994. The shape of Gaspra. Icarus 107, 23–36.

Torppa, J., Kaasalainen, M., Michalowski, T., Kwiatkowski, T., Kryszczyńska, A., Denchev, P., Kowalski, R., 2003. Shapes and rotational properties of thirty asteroids from photometric data. Icarus 164, 346–383.

van Dam, M.A., Le Mignant, D., Macintosh, B.A., 2004. Performance of the Keck Observatory Adaptive-Optics system. Appl. Opt. 43, 5458–5467.

van Houten-Groeneveld, I., van Houten, C.J., 1958. Photometrics studies of asteroids. VII. Astrophys. J. 127, 253–273.

Wang, S., Wu, Y., Bao, M., Deng, L., Wu, S., 1981. A possible satellite of 9 Metis. Icarus 46, 285–287.

Weidenschilling, S.J., Chapman, C.R., Davis, D.R., Greenberg, R., Levy, D.H., 1990. Photometric geodesy of main-belt asteroids. III. Additional lightcurves. Icarus 86, 402–447.

Wizinowich, P., Acton, D.S., Shelton, C., Stomski, P., Gathright, J., Ho, K., Lupton, W., Tsubota, K., Lai, O., Max, C., Brase, J., An, J., Avicola, K., Olivier, S., Gavel, D., Macintosh, B., Ghez, A., Larkin, J., 2000. First light adaptive optics images from the Keck II Telescope: A new era of high angular resolution imagery. Publ. Astron. Soc. Pacific 112, 315–319.

Wizinowich, P.L., Le Mignant, D., Bouchez, A.H., Campbell, R.D., Chin, J.C.Y., Contos, A.R., van Dam, M.A., Hartman, S.K., Johansson, E.M., Lafon, R.E., Lewis, H., Stomski, P.J., Summers, D.M., Brown, C.G., Danforth, P.M., Max, C.E., Pennington, D.M., 2006. The W.M. Keck Observatory Laser Guide Star Adaptive Optics system: Overview. Publ. Astron. Soc. Pacific 118, 297–309.

Worman, W.E., Fieber, S., Hulet, K., 2004. Photometry of 374 Burgundia. Minor Planet Bull. 31, 66–67.

Zappala, V., 1981. A semi-analytic method for pole determination of asteroids. Moon Planets 24, 319–325.

Zellner, N.E.B., Gibbard, S., de Pater, I., Marchis, F., Gaffey, M.J., 2005. Near-IR imaging of Asteroid 4 Vesta. Icarus 177, 190–195.